Palaeogeography, Palaeoclimatology, Palaeoecology 499 (2018) 22–34

Contents lists available at ScienceDirect

Palaeogeography, Palaeoclimatology, Palaeoecology

journal homepage: www.elsevier.com/locate/palaeo

$\delta^{18}O$ of *Fissurella maxima* as a proxy for reconstructing Early Holocene sea surface temperatures in the coastal Atacama desert (25°S)

Carola Flores[a,*], Eugenia M. Gayo[b], Diego Salazar[c], Bernardo R. Broitman[a]

[a] Centro de Estudios Avanzados en Zonas Áridas (CEAZA), Facultad de Ciencias del Mar, Universidad Católica del Norte, Ossandón 877, Coquimbo, Chile
[b] Departamento de Oceanografía, Universidad de Concepción, Centro de Ciencia del Clima y la Resilencia (CR2), Barrio Universitario s/n, Concepción, Chile
[c] Departamento de Antropología, Universidad de Chile, Ignacio Carrera Pinto 1045, Santiago, Chile

ARTICLE INFO

Keywords:
Shell carbonate
Fissurella maxima
Oxygen stable isotope
South–east Pacific coast
Temperature reconstruction
Paleotemperature calibration

ABSTRACT

Fissurella maxima is a keyhole limpet that is abundant and well preserved in archaeological shell midden sites along the coast of Chile, making it an appropriate species to use for reconstructions of past sea surface temperature (SST). In the present study we evaluate the potential of *F. maxima* shells as a proxy of SST by analysing $\delta^{18}O$ of modern shells collected alive from the Atacama desert (area of Taltal, 25°S) and archaeological shells from two Early Holocene rockshelter sites: 224A and Paposo Norte 9. Reconstructed SST from modern *F. maxima* shells were related to SST obtained from in situ thermometers, supporting the use of this mollusc species as a paleotemperature archive. Mean SST reconstructed from Early Holocene archaeological shells (14.13 °C) was 2.86 °C cooler than mean temperature recorded in modern shells (16.99 °C). Mean SST reconstructed from modern shells was ~1.04 °C warmer than the mean temperature of in situ thermometers (15.95°C). Hence the paleo–SST data from archaeological sites 224A and Paposo Norte 9 enrich the Early Holocene nearshore paleoceanographic scenario of the Pacific coast of South America, with mean SST cooler than present-day SST. Our results validate the use of *F. maxima* shells as a SST proxy and contribute to a better understanding of the latitudinal distribution of the coastal upwelling regime during the Early Holocene, temporal changes in the structure of the Humboldt Current along the Holocene, and its influence on human adaptation through the prehistory of South America.

1. Introduction

Along the west coast of temperate South America, wind–driven upwelling of deep, cold and nutrient–rich water fuels high primary productivity, which maintains some of the largest pelagic fisheries in the planet (Chavez et al., 2008). This eastern boundary upwelling ecosystem, established ~4 million years ago with the closure of the Panamanian seaway (Ibaraki, 1997), also sustains large benthic fisheries that were key for the early human inhabitants of this coastline (Latorre et al., 2017; Olguín et al., 2015a, 2015b). The large–scale spatial configuration of the wind–driven coastal upwelling regime has changed over time. Indeed, the position of the regional maxima and the sources of upwelled water experienced pronounced latitudinal changes during the Holocene (Carré et al., 2016; Kim et al., 2002; Latorre et al., 2017; Mohtadi et al., 2004; Ortlieb et al., 2011). Evidence to date suggests that the transition from the humid environmental regime of the Early Holocene to the dominantly arid coast of western South America involved a reorganization of paleoceanographic circulation patterns from southern Peru to central–northern Chile (Carré et al., 2016; Ortlieb et al., 2011). The large uncertainty around the spatial organization of these paleoceanographic changes limits proper interpretation of their effects on coastal environments and human societies in the past. Coupled studies on the isotope composition of modern and archaeological shellfish assemblages have proven to be a powerful tool for reconstructing oceanographic variability throughout the Holocene and prehistoric times (Carré et al., 2005b; Galimberti et al., 2017).

Our study aims to provide information on mean sea surface temperature (SST) during the Early Holocene using archaeological shells of *Fissurella maxima* as a paleoclimate proxy. In particular, we investigate past and present mean SST in the coastal Atacama desert (area of Taltal, 25°S) (Fig. 1), an area located halfway between southern Peru and central–northern Chile. We first calibrate the use of modern *F. maxima* (Fig. 2)–a ubiquitous mollusc in archaeological shell middens of the region–to generate a quantitative proxy for local mean SST. Subsequently, based on the relationship between SST and $\delta^{18}O$ composition in the calcium carbonate ($CaCO_3$) of *F. maxima*, we provide new information that contributes to understand better the latitudinal distribution of the coastal upwelling regime during the Early Holocene,

* Corresponding author.
E-mail addresses: carola.flores@ceaza.cl (C. Flores), emgayo@uc.cl (E.M. Gayo), dsalazar@uchile.cl (D. Salazar), bernardo.broitman@ceaza.cl (B.R. Broitman).

https://doi.org/10.1016/j.palaeo.2018.03.031
Received 22 August 2017; Received in revised form 7 March 2018; Accepted 25 March 2018
Available online 03 April 2018
0031-0182/

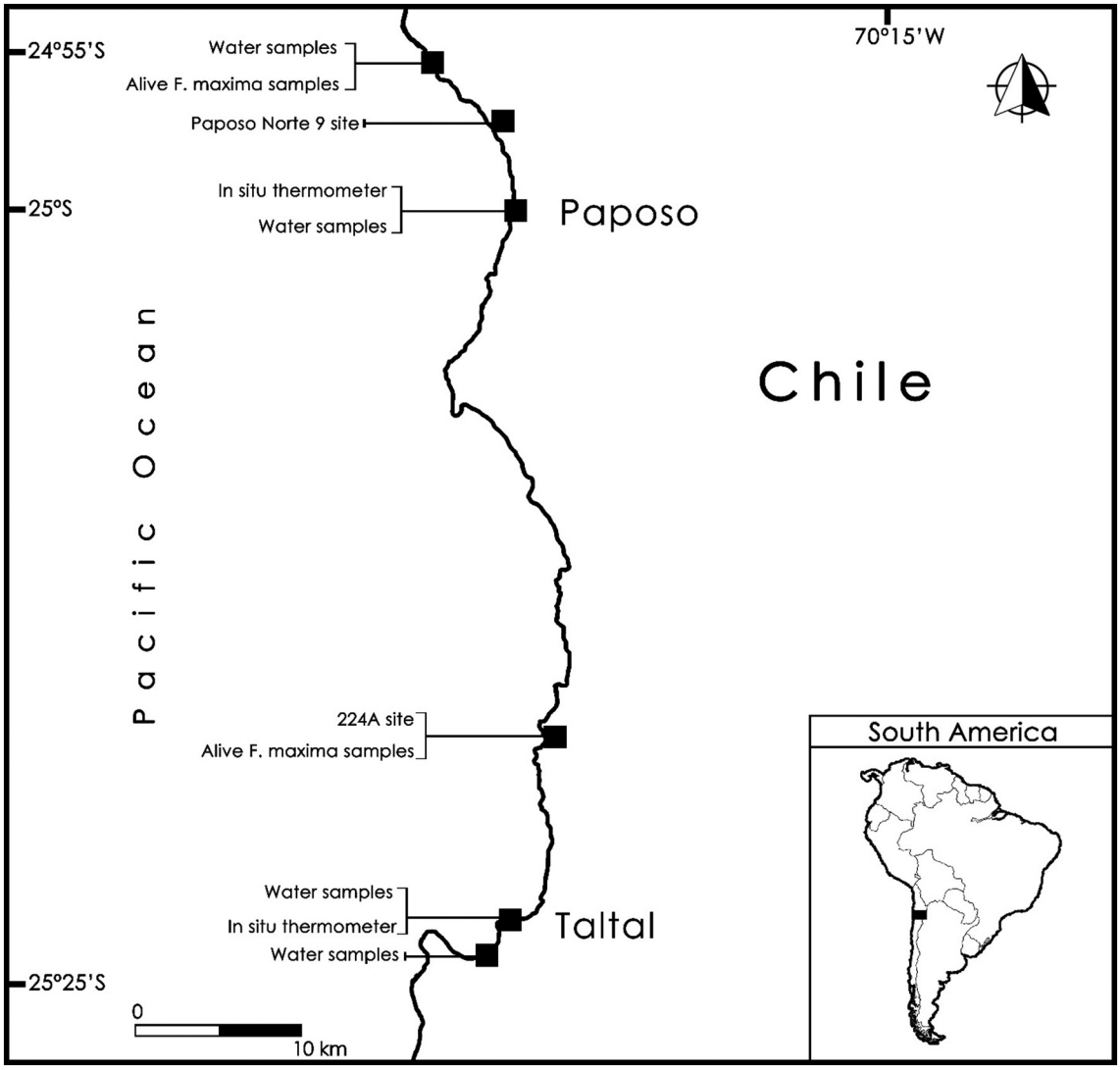

Fig. 1. Map of the study area showing places of collection of sea water samples and alive specimens of *F. maxima*, archaeological sites where shells of *F. maxima* were obtained, and location of in situ thermometers.

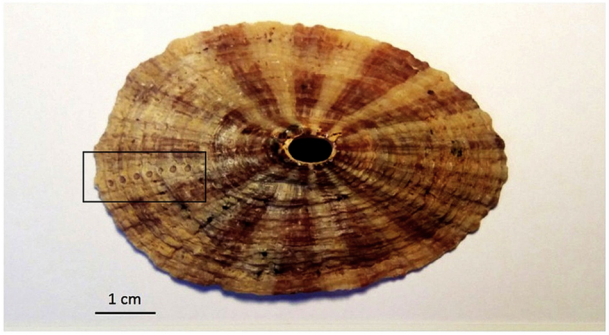

Fig. 2. *F. maxima* shell. The square marks carbonate microsamples.

temporal changes in the structure of the Humboldt Current along the Holocene, and its influence on human adaptation in the prehistory of South America.

2. Research background

Oxygen isotope ratios in mollusc $CaCO_3$ have been widely used to characterize past nearshore oceanographic conditions, particularly to reconstruct SST patterns (e.g. Carré et al., 2012; Colonese et al., 2012; Glassow et al., 2012; Jew et al., 2016; Mannino et al., 2008; Prendergast and Schöne, 2017; Surge and Barrett, 2012). As molluscs grow, they deposit new shell layers by precipitating $CaCO_3$ from seawater (Wefer and Berger, 1991). However, only some species deposit biogenic $CaCO_3$ with $\delta^{13}C$ and $\delta^{18}O$ concentrations in equilibrium with water temperature. Biological factors (i.e. ontogeny or physiology) may disrupt the predictable linear relationship between SST, oxygen composition of seawater and biogenic carbonates (Bijma et al., 1999; Ford et al., 2010; McConnaughey, 1989). This implies that paleotemperature inferences from $\delta^{18}O_{shells}$ could be biased by kinetic and vital effects, leading to an offset between $\delta^{18}O_{shell}$ and $\delta^{18}O_{water}$.

Isotope studies of shells of coastal molluscs from archaeological sites along the south-eastern Pacific have been carried out in a limited number of sites. These studies have focused on the surf clam *Mesodesma donacium* from the southern coast of Peru (18°S) (Carré et al., 2014) and central Chile (31°S) (Carré et al., 2012), and on the whelk *Concholepas concholepas* from northern (23°S) (Vargas et al., 2006) and central Chile (33°S) (Falabella et al., 1991). Regarding nearshore SST reconstructions from the Early Holocene, cooler than present SST has been inferred for northern Chile (23°S) between 10,550 and 9120 cal yr BP (Vargas et al., 2006) and slightly cooler or similar than modern SST values have been obtained from central Chile (31°S), dated between 10,380 and

9460 cal yr BP (Carré et al., 2012). This paleoceanographic pattern, complemented with studies on ^{14}C reservoir ages, has been interpreted as the result of a latitudinal gradient in upwelling intensity along the Pacific coast of South America (Carré et al., 2014, 2016; Fontugne et al., 2004; Ortlieb et al., 2011).

Studies on modern marine ecosystems indicate that variations in coastal upwelling circulation lead to strong differences in productivity and abundance of marine resources over short spatial scales (i.e. tens of km, Broitman et al., 2001; Nielsen and Navarrete, 2004; Valdivia et al., 2013). Because pre-Hispanic populations that inhabited the Pacific coast of South America relied heavily on marine resources, marine productivity variation driven by oceanographic processes might have affected cultural trajectories, consumption and gathering patterns (e.g. Santoro et al., 2017). Archaeological evidence from the Peru–Chile region shows consistent changes in fishing–gathering strategies during the Holocene (Béarez et al., 2016; Olguín et al., 2014, 2015b; Rebolledo et al., 2016; Reitz et al., 2015, 2016; Salazar et al., 2015). For instance, Early Holocene archaeological sites (12000–10,000 cal yr BP) from southern Peru and the Taltal area show fish assemblages with low mean trophic level and composed mostly of cold–tolerant species. On the other hand, in sites dated later than 8500 cal yr BP the abundance of fish remains increases considerably, together with an increment of warm–tolerant species and a diversification in fish trophic levels, including pelagic predators (i.e. *Thyrites atun*) and open–sea taxa (i.e. *Xiphias gladius*, *Kajikia audax*) (Béarez et al., 2016; Olguín et al., 2014; Rebolledo et al., 2016; Reitz et al., 2015, 2016; Salazar et al., 2015).

3. Study area and environmental setting

The study area is located on the southern coast of the Atacama desert (Fig. 1), which encompasses vast areas with virtually no rain (< 1 mm/yr) and lacking superficial hydrological resources (perennial rivers) (Houston, 2006). The core of this extreme landscape is currently located between 22 and 25°S, where vegetation is almost absent except for isolated fog–driven coastal vegetation formations on the western slopes of the Coast Range (Arroyo et al., 1988; Marquet et al., 1998; Rundel et al., 1991) and around scattered brackish springs along the coastal platform (Herrera and Custodio, 2014; Herrera et al., 2018). Moisture sources include the coastal fog locally known as "*camanchaca*" (Cereceda et al., 2008; Garreaud et al., 2008; Rundel et al., 1991) and summer coastal rains during strong El Niño years (Garreaud et al., 2003). These occasional but intense rainfall events are usually short–-lived (~1–2 days) (Wilcox et al., 2016), so it is unlikely that they affect the isotopic composition of nearshore sea waters. The topography of the coastal Atacama desert is characterized by narrow coastal terraces (~500 m wide) with steep slopes from the coast to 2000 m above sea level. Extreme marine and littoral productivity along this coast (Montecino et al., 2005; Thiel et al., 2007), is modulated by oceanographic factors such as ENSO (El Niño Southern Oscillation, cycle of warming and cooling events over the equatorial Pacific Ocean) variability and local upwelling intensity around headlands (Barber and Chavez, 1983; Chavez et al., 2008).

4. Biology and ecology of *F. maxima*

F. maxima (Sowerby 1833–1835) (Fig. 2) is an eastern south Pacific keyhole limpet, common on rocky shores between southern Peru (10°S) and central Chile (36°S) (Bretos, 1982; Bretos et al., 1983). This species inhabits the low intertidal and upper subtidal zones down to 5m. depth, below stands of kelp of the genus *Lessonia*, which is a common part of the diet of *F. maxima* (McLean, 1984; Osorio et al., 1988). They can live between 7 and 10 years, reaching 50 mm in ca. 2 years (Bretos, 1982). Mature (reproductive) specimens are 48–65 mm long, with maximum adult size ranging from 80 to 135 mm long (McLean, 1984). Metabolic activity is strongly influenced by seasonal conditions, especially ocean water temperature. Reproductive periods (spawning) are in late November–December (end of spring) and July–August (winter) (Bretos et al., 1983; McLean, 1984). Most molluscs respond to seasonal processes by slowing down or arresting growth during periods of increased metabolic demand (Schöne, 2008; Wilbur and Owen, 1964). Therefore, despite the lack of studies on the effect of changes in water temperature on the performance of *F. maxima*, it is likely that this keyhole limpet slows growth during spawning periods at the end of spring and during winter (Bretos et al., 1983; McLean, 1984).

5. Material and methods

5.1. Shell sampling and processing

Eight modern specimens of *F. maxima* were collected alive during spring 2015 (November), summer 2016 (February) and spring 2016 (November) from the surf area of rocky shores at two locations. Shell sizes ranged from 62 to 101 mm total length (measured between anterior and posterior shell edge (Jerardino and Navarro, 2008)). Four shells were collected near Taltal and four shells near Paposo, at the southern and northern limits of our study area, respectively (Fig. 1).

Archaeological shells of *F. maxima* were collected from rockshelter site 224A and Paposo Norte 9 (Fig. 1), with four shells collected at each archaeological site from stratigraphic layers associated with their earliest occupations. These sites show Early Holocene deposits from 20 to 40 cm thick with evidence of residential refuse located both inside and outside the rockshelter's drip line. Hearths are intersected with middens or ash layers containing mollusc shells, fish, bird and mammal bones, as well as lithic debris and tools, attesting to the cultural origins of the deposits (Salazar et al., 2013, 2015, 2017). Shellfish remains from these two archaeological sites contained high abundance of limpet shells throughout their occupation (Olguín et al., 2015a).

Early Holocene deposits from archaeological rockshelter site 224A have been dated between 12,426 and 10,263 cal yr BP based on three radiocarbon determinations of charcoal and shell samples. This site is located in the western foothills of the Coast Range near the current mouth of the Cascabeles Ravine, 12 km north of the city of Taltal and < 300 m from today's coastline (Salazar et al., 2015, 2017). The archaeological rockshelter site of Paposo Norte 9, with dates ranging between 11,250 and 10,566 cal yr BP (on charcoal samples), is located nearly 60 km north of Taltal and around of 200 m from the current coastline (Salazar et al., 2015, 2017).

The chronological constraint of *F. maxima* shells sampled from each archaeological site was assigned by considering the stratigraphic association between these shells and the age of the nearest dated material. Sampled shells of the three radiocarbon dates from site 224A have an associated date of 11,010 cal yr BP (10,530 ± 30 ^{14}C yr BP, Salazar et al., 2017). The associated date of shell samples retrieved from the rockshelter site Paposo Norte 9 is 11,206 cal yr BP (9813 ± 37 ^{14}C yr BP, Salazar et al., 2017).

Prior to sample extraction for isotope analysis, modern and archaeological shells were scraped to remove any organic material from the outer shell layer, then individually rinsed in deionized water and subsequently etched with muriatic acid (HCL 0.2 N) to remove diagenetically altered carbonate (Bailey et al., 1983). Finally, modern and archaeological shells were dried at 85 °C, and microsamples were collected every two millimeters (including sampling holes) along their growth axis, with eight samples taken along a ~20 mm transect from the edge of each shell towards the apical aperture. This procedure was chosen following previous studies done in California and the Caribbean (Flores, 2017; Glassow et al., 2012; Jew et al., 2016; Thakar, 2016) (Fig. 2). A total of 128 shell carbonate samples were obtained from archaeological and modern shells. Samples were drilled manually with a Foredom flexible shaft motor drill linked to a Dremel micro motor, using a 0.5 mm carbide bit. Each drill hole was about 0.5 mm in diameter and yielded 20–90 μg of powdered shell carbonate. The drill bit was cleaned in an ethanol bath and the shell was cleaned with

compressed air between samplings in order to avoid cross–contamination. Samples of powdered carbonate were analysed in the Stable Isotope Facility at the University of California, Davis. Instrument precision (1σ) is estimated as ± 0.03‰ for $\delta^{13}C$ and ± 0.05‰ for $\delta^{18}O$ and their values are expressed in relation to the international Vienna Pee Dee Belemnite (VPDB) scale.

Kinetic isotope fractionation can influence carbonate deposition in shells by inducing depleted values of both $\delta^{13}C$ and $\delta^{18}O$ in comparison to seawater (Fenger et al., 2007; McConnaughey, 1989). The simultaneous depletion of ^{13}C and ^{18}O isotopes leads to a quasi–linear relationship between $\delta^{18}O$ and $\delta^{13}C$ values in shells during the calcification processes (McConnaughey, 1989). Therefore if no correlation is found between $\delta^{18}O$ and $\delta^{13}C$ values in a shell, kinetic isotope effects were minimum during shell formation. Hence in order to evaluate the kinetic effect on the formation of modern and archaeological *F. maxima* shells from the study area, a Pearson correlation analysis was performed for $\delta^{13}C$ and $\delta^{18}O$ values of each carbonate microsample.

The vital effect can influence paleotemperature inferences from $\delta^{18}O_{shells}$, leading to an offset between $\delta^{18}O_{shell}$ and $\delta^{18}O_{water}$ (Bijma et al., 1999; Ford et al., 2010; McConnaughey, 1989). Because inter or intraspecific biological factors (e.g. ontogeny, calcification rates) that might disrupt the predictable linear relationship between SST, oxygen composition of seawater and biogenic carbonate are species-specific (Fenger et al., 2007; Ferguson et al., 2011; Ford et al., 2010; Gutiérrez-Zugasti et al., 2017; Owen et al., 2002; Prendergast et al., 2013; Prendergast and Schöne, 2017; Schifano and Censi, 1983), it is necessary to evaluate the presence of a vital effect in the deposition of *F. maxima* shells.

We tackled this issue by computing the offset from isotopic equilibrium following the procedure presented in Gutiérrez-Zugasti et al. (2017). A comparison was made between $\delta^{18}O_{shell}$ values from the edge of each modern *F. maxima* shell and the predicted $\delta^{18}O_{shell}$ calculated from seawater temperatures and $\delta^{18}O_{seawater}$. Predicted values were calculated considering averaged SST recorded at the Taltal and Paposo areas for the 4 months previous to shell collection (November 2015, February 2016 and November 2016. Table 2), and $\delta^{18}O_{seawater}$ resulting from the mean of measurements available per area in November 2015 and February 2016 (Table 1). Since information on local seawater isotope-oxygen composition was not available for November 2016, we used $\delta^{18}O_{seawater}$ for the preceding 2015 spring season. The equation of Friedman and O'Neil (1997) for calcite (Eq. (1)) was applied to interconvert $\delta^{18}O_{shell}$ values between PDB and SMOW.

$$\delta^{18}O_{SMOW} = 1.03086(\delta^{18}O_{PDB}) + 30.86 \quad (1)$$

Subsequently, the Friedman and O'Neil (1977) equations for calcite (Eq. (2)) and water (Eq. (2)) were used to calculate predicted $\delta^{18}O_{shell}$ values.

$$1000 \ln\alpha = 2.78 \times 10^6 = T^2 - 2.89 \quad (2)$$

where T is the temperature measured in degrees Kelvin and α is the fractionation between water and calcite described by the equation:

$$\alpha = (1000 + \delta^{18}O_{shell}\,(SMOW))/(1000 + \delta^{18}O_{water}\,(SMOW)) \quad [3]$$

5.2. Environmental parameters

Monthly mean SST records obtained from self–contained submersible temperature dataloggers (HOBO U22, Onet Corp., Ma USA) attached to local pier pilings in Taltal and Paposo (Fig. 1) were used to characterize the seasonal SST cycle in the study area. The accuracy of HOBO U22 water temperature loggers is ± 0.20 °C. These in situ thermometers were located approximately 1 m below mean lower low water (MLLW) and recorded water temperature every 10 min during three years from January 2013 to December 2016.

To provide a broader overview of ocean temperature conditions across the study area we used night time level–3, 8–day, 16 km^2 satellite SST from the Moderate Resolution Imaging Spectroradiometer (MODIS) imagery downloaded from the NASA website (http://oceancolor.gsfc.nasa.gov/). Over a period overlapping the in situ thermometer SST records described above, we calculated the monthly mean satellite SST of the coastal zone between Paposo and Taltal by averaging between images with > 80% valid pixels over an area extending 24 km offshore and 48 km alongshore (e.g. 288 km^2, white square in Fig. 4).

To characterize the isotope composition of local sea water ($\delta^{18}O_{water}$ and δ_2H_{water}) we collected eight 5 ml samples from the shore in November 2015 and eight in February 2016 from Taltal and Paposo (Fig. 1). At each location, sea water samples were obtained from the surf zone and from fishing wharves. The oxygen and hydrogen isotope composition of these samples was analysed at the Isotope Biogeochemistry Laboratory, Department of Oceanography, University of Concepcion, using a Picarro L2130-*i* Analyser. The results obtained were normalized to the *Vienna Standard Mean Ocean Water* (*VSMOW*) scale through repeated analysis of 4 laboratory working standards calibrated relative to VSMOW: distilled water ($\delta^{18}O = -13.32‰ \pm 0.02‰$, $\delta^{2}H = -84.41‰ \pm 0.10‰$), snow ($\delta^{18}O = -12.61‰ \pm 0.02‰$, $\delta^{2}H = -102.17‰ \pm 0.09‰$), sea water ($\delta^{18}O = -0.34‰ \pm 0.05$, ‰, $\delta^{2}H = +0.88‰ \pm 0.17‰$) and mineral water ($\delta^{18}O = -13.17‰ \pm 0.03‰$, $\delta^{2}H = -96.66‰ \pm 0.08‰$).

Table 1
Seawater $\delta^{18}O$ values obtained from samples collected at Taltal and Paposo.[a]

Code	Area of collection	UTM North	UTM East	Season of collection	Month of collection	Year	$\delta^{18}O_{VSMOW}$/‰	S.D.	$\delta^{2}H_{VSMOW}$/‰	S.D.
P1	Taltal	7,189,875	351,172	Spring	November	2015	−0.50	0.03	+0.3	0.11
P2	Taltal	7,189,875	351,172	Spring	November	2015	−0.31	0.03	+0.8	0.08
P3	Paposo	7,233,255	351,793	Spring	November	2015	+0.28	0.06	+2.9	0.18
P4	Paposo	7,233,255	351,793	Spring	November	2015	+0.48	0.02	+3.6	0.11
P15	Paposo	7,242,020	346,816	Spring	November	2015	+0.74	0.03	+4.3	0.06
P16	Paposo	7,242,020	346,816	Spring	November	2015	−0.35	0.03	+1.3	0.07
P8	Taltal	7,190,974	351,839	Spring	November	2015	−0.37	0.06	+0.8	0.10
P9	Taltal	7,190,974	351,839	Spring	November	2015	+0.13	0.20	+2.7	0.36
P5	Paposo	7,242,020	346,816	Summer	February	2016	−0.35	0.04	+1.3	0.17
P6	Paposo	7,242,020	346,816	Summer	February	2016	−0.21	0.13	+1.4	0.18
P12	Paposo	7,233,255	351,793	Summer	February	2016	+0.57	0.03	+4.1	0.18
P14	Paposo	7,233,255	351,793	Summer	February	2016	−0.20	0.02	+1.9	0.11
P7	Taltal	7,189,135	350,154	Summer	February	2016	+0.07	0.05	+1.9	0.32
P10	Taltal	7,189,135	350,154	Summer	February	2016	−0.21	0.02	+1.5	0.14
P11	Taltal	7,191,004	351,776	Summer	February	2016	+0.02	0.05	+2.3	0.12
P13	Taltal	7,191,004	351,776	Summer	February	2016	+0.00	0.02	+2.4	0.05
MEAN							−0.01	0.05		

[a] Sampling places geo—referenced in Universal Transverse Mercator (UTM) (WSG 84).

5.3. $\delta^{18}O_{shell}$ and reconstructed temperatures

In order to use the correct carbonate temperature equation to reconstruct water temperature we assessed the carbonate composition (calcite vs. aragonite) of *F. maxima* shells. Results of X–Ray diffractometry (XRD) analyses on one modern *F. maxima* shell showed that calcium carbonate of its inner and outer shell layers were composed of aragonite and calcite, respectively, which matches with a previous study on *Fissurella crassa* (Boogild, 1930 in McLean, 1984). Hence, while collecting carbonate samples from modern and archaeological shells, care was taken to ensure that drilled holes did not penetrate into the inner layer of the shell (Keith et al., 1964). XRD analyses were done at the Institute of Applied Economic Geology, University of Concepción, Chile using a BRUKER D4 equipped with a Lynxeye detector and operated with Cu radiation with a filter of Ni K beta radiation.

Previous SST reconstructions for southern Peru and north–central Chile have used different equations to translate $\delta^{18}O_{shell}$ into SST (Carré et al., 2005a, 2005b, 2012). The equations employed by Carré et al. (2005b) and Grossman and Ku (1986) are appropriate for shells with calcium carbonate composed of aragonite (e.g. *M. donacium)*. Equations for calcite have not been used along the coast of South America except for a study in the Beagle Channel, southern Patagonia, based on limpet shells (*Nacella deaurata* and *N. maguellanica*) (Colonese et al., 2012), which used the calcite equation originally proposed by Wanamaker Jr. et al. (2007) for a north Atlantic (Greenland) mussel species (*Mytilus edulis*).

We chose for our study the carbonate temperature equation (Eq. (4)) developed by Ford et al., (2010) for *Mytilus californianus* from the northeastern Pacific (California). This mussel species has a shell composed of calcite, like *F. maxima*. The conversion of $\delta^{18}O_{shell}$ signature into paleoSST was calculated as follows:

$$1000\ \ln((1000 + \delta^{18}O_{equilibrium\ calcite})/(1000 + \delta^{18}O_{seawater})) = 18.734\,(10^3\ T^{-1}) - 33.776 \quad (4)$$

where T is temperature in degrees Kelvin, isotope values of sea water are reported relative to Standard Mean Ocean Water (SMOW) and isotope values of calcite are reported relative to Vienna PeeDee Belemnite (VPDB). To convert Kelvin to Celsius we subtracted 273.15 from SST values. The $\delta^{18}O_{seawater}$ value used in the equation corresponds to the mean value of local measurements of sea water obtained from the Taltal and Paposo areas (Fig. 1, Table 1). Given that our shell sampling strategy does not control for shell growth rates or chronology of shell microsamples, it was not possible to calculate the slope of the regression line between instrumental SST and $\delta^{18}O_{shell} - \delta^{18}O_{seawater}$ of each shell microsample. Also, as variation in growth rate of sampled *F. maxima* may over or underestimate the slope, it is not possible to test the slope of the Ford et al. (2010) equation. Consequently, sea surface temperature calculation of modern and archaeological $\delta^{18}O_{shell}$ values was carried out using the slope provided by Eq. (4) (Ford et al., 2010).

Temporal fluctuations in the extension of global ice sheets influence $^{18}O/^{16}O$ ratios of seawater and thus $^{18}O/^{16}O$ ratios in carbonate micro and macrofossils like marine mollusc shells (Aharon and Chappell, 1986; Duplessy et al., 2002). Archaeological shells used for this study come from two Early Holocene rockshelter sites dated between 12,426 and 10,566 cal yr BP. During this time there were still some remains of glacial ice sheets, so higher than present $\delta^{18}O_{seawater}$ values are expected. To account for the ice volume effect on sea water $\delta^{18}O$, an ice volume correction of −0.463‰ was applied to $\delta^{18}O$ values of shells from site 224A based on their associated date of 11,010 cal yr BP. The correction for $\delta^{18}O$ values of shells from Paposo Norte 9 site was −0.445‰ based on the associated date of 11,206 cal yr BP. Correction values were calculated using the sea level reconstruction from Lambeck and Chappell (2001) and a maximum ice volume effect of 1.05‰ for the last glacial maximum (LGM) (Duplessy et al., 2002).

$$\text{Ice volume correction} = (\text{sl}/145) \times 1.05 \quad (5)$$

where sl is the global sea level for the time period under study (Lambeck and Chappell, 2001) divided by the lowest sea level recorded from the period between last glacial maximum to the end of major ice sheet decay (preset time) (Lambeck and Chappell, 2001), and then multiplied by the difference of seawater $\delta^{18}O$ values between LGM and today (Duplessy et al., 2002).

6. Results

6.1. Environmental parameters

Continuous thermometer SST records at Taltal and Paposo indicated a long–term mean of 15.95 °C with a range of 3.75 °C between the warmest (mean of 18 °C, summer, February 2016) and coolest month (mean of 14.25 °C, spring, September 2014) (Fig. 3, Table 2). Satellite SST for the coastal zone of the study area indicates a long–term mean SST of 16.88 °C, with a range of 6.51 °C between the warmest (mean of 20.76 °C, summer, February 2016) and coolest month (mean of 14.25 °C, winter, August 2013) (Fig. 4, Table 3). The Pearson correlation between monthly SST values from thermometers and satellite measurements for the coastal area between Paposo and Taltal (Fig. 4) was strong and highly significant (r = 0.778, p = 0.000), with satellite SST values consistently ~1–2 °C warmer than in situ records (Fig. 5, Fig. 6).

A mean $\delta^{18}O_{seawater}$ value of −0.01 ± 0.05‰ was obtained from 16 water samples collected at Taltal and Paposo during November 2015 and February 2016 (Table 1). Seasonal mean values did not differ significantly between spring (+0.01 ± 0.46‰) and summer (−0.04 ± 0.29‰) (Mann-Whitney U = 30.50, p = 0.91) (Table 1). Mean $\delta^{18}O_{seawater}$ values for both seasons closely followed the average value for the surface ocean, but were slightly lower than the southern Peruvian coast (0.13–0.16‰, Carré et al., 2005b, 2012).

6.2. Shell oxygen isotopes ($\delta^{18}O_{shell}$)

To evaluate the kinetic effect on the formation of modern and archaeological *F. maxima* shells, a Pearson correlation analysis was performed for $\delta^{13}C$ and $\delta^{18}O$ values of modern and archaeological carbonate microsamples. For the 64 microsamples of modern *F. maxima* shells, a non–significant relationship (r = 0.273, p = 0.029) was found between their $\delta^{13}C$ and $\delta^{18}O$ values (raw values in Supplementary Data

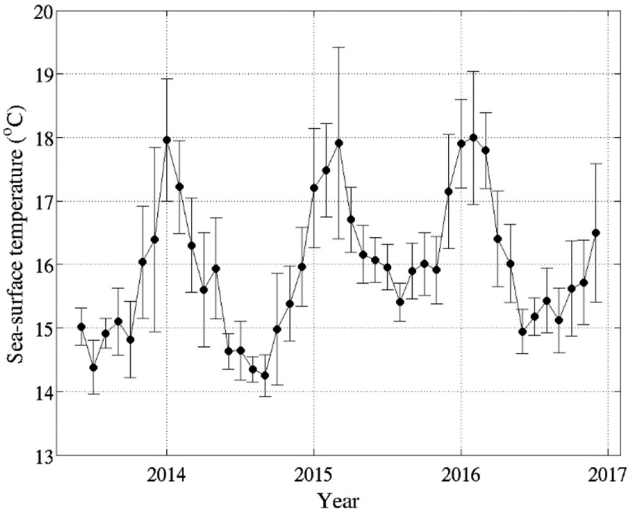

Fig. 3. Monthly mean sea surface temperature record for the study area from in situ thermometers at Paposo and Taltal from 2013 to 2016. Error bars represent one standard deviation.

Table 2
Monthly mean SST (°C) from in situ thermometers at Taltal and Paposo.

Year	Month	SST (°C)					
		Mean	Median	Max	Min	S.D.	Var
2013	June	15.02	15.08	15.56	14.15	0.29	0.09
2013	July	14.38	14.47	15.01	13.23	0.42	0.18
2013	August	14.92	14.92	15.32	14.29	0.24	0.06
2013	September	15.10	15.13	16.01	13.86	0.53	0.28
2013	October	14.82	14.94	15.75	13.35	0.60	0.36
2013	November	16.04	15.82	17.53	14.72	0.88	0.78
2013	December	16.40	16.65	19.21	14.02	1.45	2.10
2014	January	17.96	18.10	19.70	16.27	0.96	0.92
2014	February	17.22	17.33	18.54	15.34	0.73	0.53
2014	March	16.30	16.41	17.74	15.05	0.74	0.55
2014	April	15.60	15.58	17.12	14.09	0.90	0.81
2014	May	15.94	15.91	17.47	14.63	0.80	0.64
2014	June	14.63	14.64	15.00	14.18	0.28	0.08
2014	July	14.64	14.84	15.15	13.57	0.46	0.21
2014	August	14.35	14.34	14.73	13.87	0.20	0.04
2014	September	14.25	14.33	14.98	13.67	0.33	0.11
2014	October	14.98	15.11	16.36	13.46	0.88	0.77
2014	November	15.39	15.51	16.18	14.27	0.59	0.34
2014	December	15.97	15.98	17.24	14.88	0.62	0.39
2015	January	17.20	17.12	19.27	15.35	0.94	0.88
2015	February	17.48	17.50	19.12	16.37	0.74	0.54
2015	March	17.91	17.30	20.51	15.91	1.51	2.28
2015	April	16.71	16.74	17.87	15.63	0.51	0.26
2015	May	16.16	16.22	16.99	15.31	0.45	0.21
2015	June	16.07	15.96	16.75	15.52	0.35	0.13
2015	July	15.96	15.91	16.86	15.35	0.36	0.13
2015	August	15.41	15.43	15.94	14.74	0.30	0.09
2015	September	15.90	15.90	16.99	15.02	0.44	0.19
2015	October	16.01	16.06	17.00	14.84	0.49	0.24
2015	November	15.91	15.92	17.03	15.09	0.53	0.28
2015	December	17.15	17.47	18.56	15.46	0.90	0.81
2016	January	17.90	17.87	19.45	16.75	0.70	0.48
2016	February	18.00	18.10	19.52	16.07	1.05	1.10
2016	March	17.79	17.81	19.18	16.70	0.60	0.35
2016	April	16.40	16.14	18.50	15.49	0.76	0.57
2016	May	16.02	15.95	17.26	15.08	0.62	0.38
2016	June	14.95	14.97	15.51	13.88	0.35	0.12
2016	July	15.18	15.17	15.75	14.45	0.30	0.09
2016	August	15.43	15.37	16.32	14.60	0.51	0.26
2016	September	15.12	15.07	15.97	14.06	0.51	0.26
2016	October	15.62	15.57	16.92	14.59	0.75	0.56
2016	November	15.72	15.82	16.89	13.88	0.67	0.44
2016	December	16.50	16.40	18.46	14.82	1.09	1.18
TOTAL		15.95	15.77	20.51	13.23	1.26	1.58

1), which discounts kinetic effects on the formation of modern shells. A non–significant relationship ($r = -0.170$, $p = 0.179$) was also found in carbonate microsamples of archaeological shells (raw values in Supplementary Data 1), excluding kinetic effects on the formation of these specimens.

To evaluate whether *F. maxima* precipitates its shell in isotopic equilibrium with surrounding water (vital effect), predicted and measured $\delta^{18}O_{shell}$ values from the edge of modern *F. maxima* shells were compared, obtaining a moderate inverse but non–significant correlation ($r = -0.561$, $p = 0.148$). SST and $\delta^{18}O_{water}$ data from the Paposo and Taltal areas predict $\delta^{18}O_{shell}$ values ranging from −0.51 to +0.34‰ with an average of −0.20‰ (Table 4). Measured $\delta^{18}O_{shell}$ values at the edge of modern *F. maxima* were consistently enriched, ranging from +0.44‰ to +1.06‰, mean = +0.80‰ (Table 4). This positive deviation of measured $\delta^{18}O_{shell}$ values showed high variability among modern *F. maxima* shell samples (Fig. 7), with an average offset of 1 ± 0.5‰. Despite this variability, the relationship between predicted and measured $\delta^{18}O_{shell}$ was similar in the two localities (Paposo and Taltal) and seasons (austral spring versus summer), which suggests that environmental factors are not driving the observed deviations from the isotopic equilibrium.

The average offset of 1‰ was subtracted from measured $\delta^{18}O_{shell}$ values of modern *F. maxima* shells. Mean $\delta^{18}O_{shell}$ values obtained after correction are summarized in Table 5 (raw values in Supplementary Data 1) and range between −1.20‰ and +0.06‰ (mean = +0.61‰, SD = +0.35‰). Mean $\delta^{18}O_{shell}$ values obtained from modern *F. maxima* shells without the offset correction are summarized in Table 6 (raw values in Supplementary Data 1) and range between −0.20‰ and +1.06 ‰ (mean = +0.39‰, SD = +0.35‰). Mean $\delta^{18}O_{shell}$ values from archaeological shells without the offset correction are slightly enriched in ^{18}O compared to modern counterparts, ranging from +0.00‰ to +1.72‰ (mean = +1.03‰ SD = +0.35‰) (Table 6). Microsample A.C.4.G from archaeological shell ID A.C.4. was excluded from analyses performed in this study as it yielded an outlying $\delta^{18}O$ value of +3.31‰ (raw values in Supplementary Data 1). Consequently, for the purpose of the study only seven microsamples were considered from shell ID A.C.4 and this outlier value is not included in Table 6.

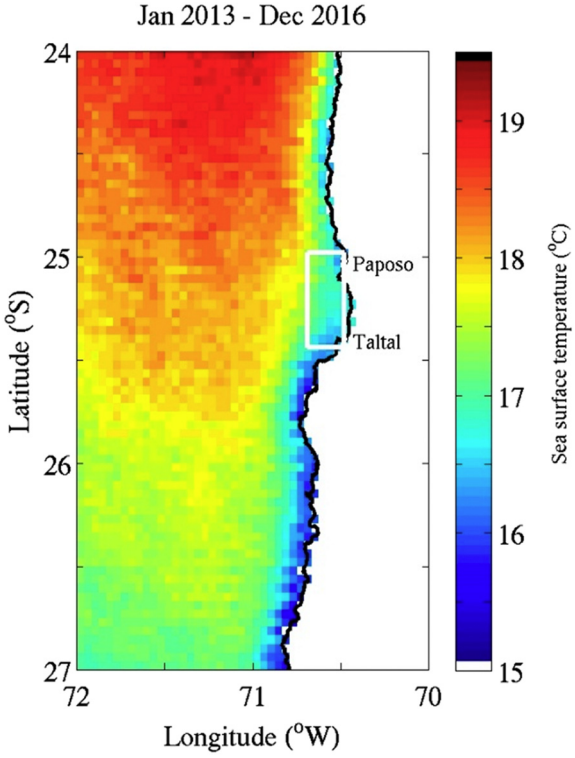

Fig. 4. Mean sea surface temperature between Paposo and Taltal recorded in satellites from 2013 to 2016. The white square indicates the area considered for satellite SST analyses.

6.3. Reconstructed temperatures

To evaluate a vital effect correction on SST reconstruction, the +1‰ offset was subtracted from modern *F. maxima* $\delta^{18}O_{shell}$ values. Corrected *F. maxima* $\delta^{18}O_{shell}$ values were then converted to SST using Eq. (4) (Ford et al., 2010); the mean SST obtained was 21.56 °C with a lower and upper mean SST value of 20.35 °C (Shell ID B.C.2) and 22.53 °C (Shell ID L.F.P.2) (Table 7). Applying the same SST Equation (Ford et al., 2010) to modern *F. maxima* $\delta^{18}O_{shell}$ values but without the offset correction, the mean SST obtained was 16.99 °C with lower and upper mean SST values of 15.82 °C (Shell ID B.C.2) and 17.93 °C (Shell ID L.F.P.2) (Table 8). Finally, using Eq. (4) and considering the ice-volume effect, mean SST from archaeological *F. maxima* $\delta^{18}O_{shell}$ values (without the offset correction) was 14.13 °C with minimum and maximum mean SST values of 13.36 °C (Shell ID A.C.2) and 15.52 °C (Shell ID P.F.4), respectively (Table 8).

Table 3
Monthly mean SST (°C) from satellite information of the area between Taltal and Paposo.

Year	Month	Mean (°C)
2013	June	16.06
2013	July	15.42
2013	August	14.25
2013	September	14.64
2013	October	14.49
2013	November	15.30
2013	December	15.98
2014	January	17.60
2014	February	19.18
2014	March	18.80
2014	April	18.62
2014	May	17.32
2014	June	17.08
2014	July	15.64
2014	August	15.16
2014	September	14.86
2014	October	14.72
2014	November	15.97
2014	December	15.97
2015	January	No info
2015	February	18.66
2015	March	19.35
2015	April	18.72
2015	May	18.25
2015	June	17.44
2015	July	15.73
2015	August	15.56
2015	September	15.70
2015	October	15.72
2015	November	15.86
2015	December	16.89
2016	January	19.33
2016	February	20.76
2016	March	19.76
2016	April	18.94
2016	May	18.19
2016	June	17.74
2016	July	15.43
2016	August	15.06
2016	September	14.72
2016	October	15.08
2016	November	15.78
2016	December	17.61
Mean		16.88

7. Discussion

To provide a correction value for SST records obtained from satellite data, we compared mean SST of the study area recorded by thermometers and satellites between January 2013 and December 2016 (Fig. 1). The correction value obtained from this comparison is relevant for cases when only satellite SST data is available for comparison with reconstructed shell SST (i.e. Ferguson et al., 2011; Flores, 2017; Glassow et al., 2012; Jew et al., 2016; Prendergast and Schöne, 2017). Mean SST recorded by satellite was 0.93 °C higher than mean SST recorded by thermometers during the three year period (Table 9). The maximum monthly mean SST recorded by satellite was 2.76 °C higher than maximum mean SST from thermometers. In contrast, the minimum monthly mean SST was 14.25 °C from both satellites and thermometers (Table 7). The 0.93 °C difference between monthly thermometer and satellite SST records was expected from the radiative effect of the adjacent landmass and is in line with reports from south-central Chile and other coastal locations worldwide (Aravena et al., 2014). The strong linear relationship between satellite and thermometer SST indicates that both sources of information provide a reliable view of SST variability over the study area (Fig. 5). Nevertheless, as mean SST recorded by satellite was 0.96 °C higher than thermometers, this difference has to be considered when using satellite estimates for mean SST.

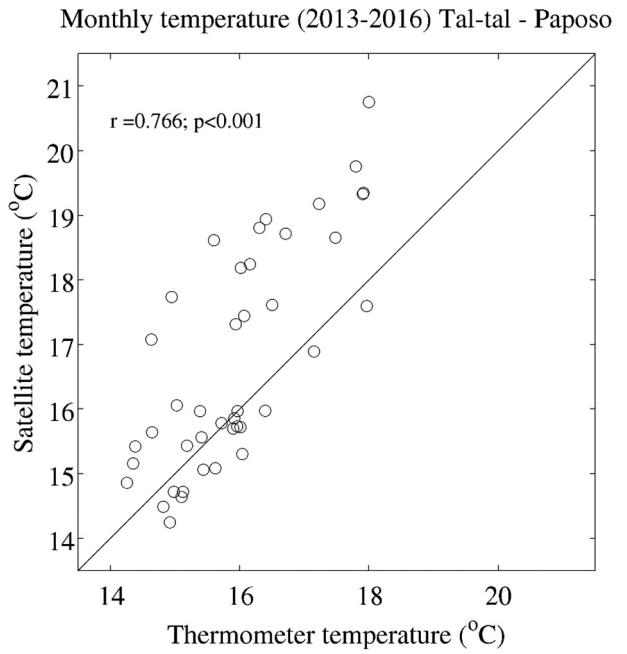

Fig. 5. Linear correlation between monthly sea surface temperature values for in situ thermometers and satellite.

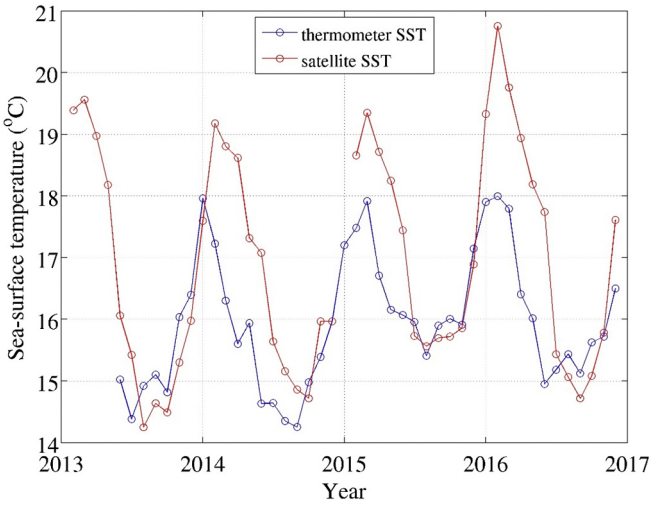

Fig. 6. Monthly mean SST records from in situ thermometers and satellite for the study area from January 2013 to December 2016.

As mentioned previously, vital effect can cause isotope disequilibrium in carbonate skeletons, which is reflected by $\delta^{18}O_{shell}$ values more positive than expected equilibrium values. The average offset estimated for modern *F. maxima* shell edges is +1 ± 0.5‰ and therefore is coherent with a positive deviation of measured $\delta^{18}O_{shell}$ values (Fig. 7). Studies on *Patella* species from different locations have shown a consistent positive offset, ranging between 0.2‰ and 1.3‰ (Cohen and Tyson, 1995; Colonese et al., 2012; Fenger et al., 2007; Ferguson et al., 2011; Gutiérrez-Zugasti et al., 2017; Parker et al., 2017; Prendergast and Schöne, 2017). The calculated offset for *F. maxima* is close to the upper limit identified in isotope studies on the limpet *Patella vulgata* (1.01‰) from the eastern coast of England (Fenger et al., 2007) and *Patella candei crenata* (1.3‰) from the Canary Islands (Parker et al., 2017).

When the offset value of 1 ± 0.5‰ is subtracted from modern *F. maxima* $\delta^{18}O_{shell}$, the reconstructed mean SST (21.56 °C ± 2.58, Table 7) is ~5.61 °C warmer than mean temperatures recorded by in

Table 4
Parameters employed to estimate isotope fractionation offset of measured $\delta^{18}O_{calcite}$ at the edge of modern *F. maxima* shells.[a]

Shell sample	Area of collection	Season of collection	Measured calcite $\delta^{18}O$ (‰. PDB)	Measured calcite $\delta^{18}O$ (‰. SMOW)	Seawater $\delta^{18}O$ (‰. SMOW)	Thermometer mean SST (°C)	Predicted calcite $\delta^{18}O$ (‰. SMOW)	Predicted calcite $\delta^{18}O$ (‰. PDB)	Offset ‰
B.C.2.A.	Taltal	November 2015	+1.02	+31.91	+0.26	16.14	+30.44	−0.41	−1.43
B.P6.2.A	Taltal	February 2016	+1.06	+31.95	−0.03	17.65	+30.33	−0.51	−1.57
Z.P6.1.A	Paposo	February 2016	+0.65	+31.53	−0.05	16.82	+30.5	−0.35	−1.00
Z.P6.2.A	Paposo	February 2016	+0.53	+31.41	−0.05	16.82	+30.5	−0.35	−0.88
B.C.P.1.A	Taltal	November 2016	+0.93	+31.82	−0.26	15.72	+30.54	−0.31	−1.24
B.C.P.2.A	Taltal	November 2016	+1.01	+31.90	−0.26	15.72	+30.54	−0.31	−1.32
L.F.P.1.A	Paposo	November 2016	+0.44	+31.31	+0.28	15.26	+31.21	+0.34	−0.10
L.F.P.2.A	Paposo	November 2016	+0.76	+31.64	+0.28	15.26	+31.21	+0.34	−0.42

[a] Modern shell samples: Letter A at the end identifies sample obtained at the edge of *F. maxima* shells.

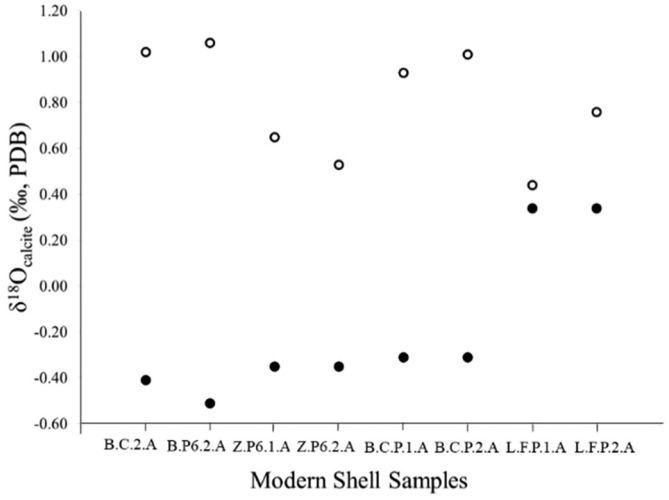

Fig. 7. Observed (open dots) versus predicted (dark dots) $\delta^{18}O_{calcite}$ values on modern *F. maxima* shells.

situ thermometers (15.95 °C ± 1.58, Table 2), and minimum and maximum mean SST values (20.53 and 22.53 °C) fall far outside the instrumental mean SST range (14.25 and 18 °C). On the other hand, when SST reconstruction is done with $\delta^{18}O_{shell}$ values without the offset correction, shell mean SST (16.99 °C ± 2.42, Table 8) was ~1.04 °C warmer than instrumental mean SST (Table 2), minimum and maximum mean SST values (15.82 and 17.93 °C) fall within instrumental mean SST range, and shell SST values record the full range of seasonal SST recorded in thermometers (see Max and Min SST values in Table 8). An explanation for the extremely high mean SST of $\delta^{18}O_{shell}$ values with the offset correction may be the low precision of data used in the vital effect calculation. Previous studies have mentioned that the greater the resolved data used for the isotopic composition of the water when calculating predicted $\delta^{18}O_{shell}$, the smaller the offset between predicted and measured values (Ferguson et al., 2011; Gutiérrez-Zugasti et al., 2017). As the size of the offset is highly sensitive to $\delta^{18}O_{seawater}$ values, our water sampling with only seasonal measurements and the use of $\delta^{18}O_{seawater}$ values from November 2015 in the calculation of shells collected during November 2016 (Table 4) may account for a source of error in our vital effect calculation. Also, there are no other isotope studies on *Fissurella* species to compare our offset and evaluate its size and direction. Moreover, the coarse shell sampling resolution used in the study does not provide information on specimen age (ontogenetic effect) or on the time interval included in each shell sample. Consequently, no specific time can be assigned to $\delta^{18}O_{shell}$ samples to link them to $\delta^{18}O_{seawater}$ signatures and perform an accurate vital effect calculation.

Regarding correlation between instrumental SST and reconstructed values from $\delta^{18}O_{shell}$ on modern shells, previous studies have found a closer correspondence between both estimates. These studies have performed oxygen isotope analyses on different mollusc species. For instance, mean SST reconstruction on *Patella vulgata* for the northern coast of Spain yielded values 0.40–0.90 °C cooler than instrumental records (Gutiérrez–Zugasti et al., 2017). Mean SST from opercula and shell carbonate of *T. sarmaticus* from the coast of South Africa, was also 0.40 °C colder than instrumental mean SST (Galimberti et al., 2017). A study on *M. donacium* found a strong correlation between measured SST and shell SST (Carré et al., 2005b). Finally, reconstructed SST for *N. deaurata* and *N. maguellanica* shells from the Beagle Channel showed that shell average SST was around 0.50 °C below SST instrumentally recorded from the study area (Colonese et al., 2012). Reconstructed mean SST for *F. maxima* ($\delta^{18}O_{shell}$ values without the offset correction)

Table 5
Reported $\delta^{18}O_{shellVPDB}$/‰ from modern *F. maxima* shells after subtracting 1 ± 0.5‰ to account for the vital effect.[a]

Shell ID	Type	Area of collection	Date of collection	N	UTM north	UTM east	$\delta^{18}O_{VPDB}$/‰					
							Mean	Median	Max	Min	S.D.	Var
B.C.2	Modern	Taltal area	November 2015	8	7,200,553	353,748	−0.35	−0.27	+0.03	−1.00	0.36	0.13
B.P6.2	Modern	Taltal area	February 2016	8	7,200,553	353,748	−0.51	−0.50	+0.06	−0.99	0.37	0.14
Z.P6.1	Modern	Paposo area	February 2016	8	7,242,032	346,788	−0.49	−0.51	−0.19	−0.76	0.21	0.04
Z.P6.2	Modern	Paposo area	February 2016	8	7,242,032	346,788	−0.48	−0.45	−0.01	−0.89	0.32	0.10
B.C.P.1	Modern	Taltal area	November 2016	8	7,200,553	353,748	−0.68	−0.80	−0.05	−1.19	0.43	0.18
B.C.P.2	Modern	Taltal area	November 2016	8	7,200,553	353,748	−0.79	−0.90	+0.01	−1.11	0.36	0.13
L.F.P.1	Modern	Paposo area	November 2016	8	7,242,032	346,788	−0.77	−0.80	−0.56	−0.93	0.16	0.03
L.F.P.2	Modern	Paposo area	November 2016	8	7,242,032	346,788	−0.82	−0.81	−0.24	−1.20	0.29	0.08
Total modern							−0.61	−0.68	+0.06	−1.20	0.35	0.12

[a] N refers to the number of samples per shell.

Table 6
Reported $\delta^{18}O_{shellVPDB}$/‰ from modern and archaeological *F. maxima* shells without vital effect correction.[a]

Shell ID	Type	Area of collection	Date of collection	N	UTM north	UTM east	$\delta^{18}O_{VPDB}$/‰					
							Mean	Median	Max	Min	S.D.	Var
B.C.2	Modern	Taltal area	November 2015	8	7,200,553	353,748	+0.65	+0.73	+1.03	+0.00	0.36	0.13
B·P6.2	Modern	Taltal area	February 2016	8	7,200,553	353,748	+0.49	+0.50	+1.06	+0.01	0.37	0.14
Z.P6.1	Modern	Paposo area	February 2016	8	7,242,032	346,788	+0.51	+0.49	+0.81	+0.24	0.21	0.04
Z.P6.2	Modern	Paposo area	February 2016	8	7,242,032	346,788	+0.52	+0.55	+0.99	+0.11	0.32	0.10
B.C.P.1	Modern	Taltal area	November 2016	8	7,200,553	353,748	+0.32	+0.20	+0.95	−0.19	0.43	0.18
B.C.P.2	Modern	Taltal area	November 2016	8	7,200,553	353,748	+0.21	+0.10	+1.01	−0.11	0.36	0.13
L.F.P.1	Modern	Paposo area	November 2016	8	7,242,032	346,788	+0.23	+0.20	+0.44	+0.07	0.16	0.03
L.F.P.2	Modern	Paposo area	November 2016	8	7,242,032	346,788	+0.18	+0.19	+0.76	−0.20	0.29	0.08
Total modern							+0.39	+0.32	+1.06	−0.20	0.35	0.12
A.C.1	Archaeological	Site 224A	10,995 cal yr BP	8	7,201,935	354,249	+1.19	+1.17	+1.72	+0.83	0.33	0.11
A.C.2	Archaeological	Site 224A	10,995 cal yr BP	8	7,201,935	354,249	+1.21	+1.18	+1.68	+0.86	0.25	0.06
A.C.3	Archaeological	Site 224A	10,995 cal yr BP	8	7,201,935	354,249	+1.17	+1.24	+1.48	+0.78	0.28	0.08
A.C.4	Archaeological	Site 224A	10,995 cal yr BP	7	7,201,935	354,249	+1.07	+0.94	+1.51	+0.80	0.29	0.08
P.F.1	Archaeological	Site PN9	11,210 cal yr BP	8	7,238,590	350,569	+0.95	+0.84	+1.55	+0.67	0.29	0.08
P.F.2	Archaeological	Site PN9	11,210 cal yr BP	8	7,238,590	350,569	+1.14	+1.09	+1.53	+0.84	0.25	0.06
P.F.3	Archaeological	Site PN9	11,210 cal yr BP	8	7,238,590	350,569	+0.83	+0.77	+1.70	+0.29	0.44	0.20
P.F.4	Archaeological	Site PN9	11,210 cal yr BP	8	7,238,590	350,569	+0.72	+0.70	+1.46	+0.00	0.43	0.19
Total archaeological							+1.03	+1.01	+1.72	+0.00	0.35	0.13

[a] N refers to the number of samples per shell.

Table 7
Reconstructed SST (°C) from modern *F. maxima* shells with Vital Effect correction.[a]

Shell ID	Type	Site of collection	n	SST (°C)					
				Mean	Median	Max	Min	S.D.	Var
B.C.2	Modern	Taltal area	8	20.35	20.00	23.37	18.64	1.65	2.71
B·P6.2	Modern	Taltal area	8	21.08	21.06	23.31	18.49	1.72	2.95
Z.P6.1	Modern	Paposo area	8	21.01	21.08	22.24	19.61	0.95	0.90
Z.P6.2	Modern	Paposo area	8	20.94	20.81	22.85	18.78	1.49	2.23
B.C.P.1	Modern	Taltal area	8	21.91	22.43	24.29	18.97	1.97	3.89
B.C.P.2	Modern	Taltal area	8	22.40	22.91	23.87	18.71	1.68	2.82
L.F.P.1	Modern	Paposo area	8	22.29	22.43	23.07	21.31	0.74	0.55
L.F.P.2	Modern	Paposo area	8	22.53	22.49	24.32	19.83	1.35	1.82
Total modern				21.56	21.87	24.32	18.49	1.61	2.58

[a] N refers to the number of samples per shell.

Table 9
SST (°C) from in situ thermometers, satellite imagery, archaeological *F. maxima* shells and modern *F. maxima* shells.[a]

SST (°C)	Thermometers	Satellite	Modern *F. maxima* Shell	Modern *F. maxima* shell (co)	Archaeological *F. maxima* shell
Mean	15.95	16.88	16.99	21.56	14.13
Maximum mean	18.00	20.76	17.93	22.53	15.52
Minimum mean	14.25	14.25	15.82	20.35	13.56
Range	3.75	6.51	2.11	2.18	1.96

[a] (co) indicates SST information on corrected $\delta^{18}O_{shell}$ values from vital effect.

was ~1.04 °C warmer than instrumental SST, over representing mean water temperature and differing from what has been found for most *Patella* species. One exception is *Patella caerulea* from the

Table 8
Reconstructed SST (°C) from modern and archaeological *F. maxima* shells without vital effect correction.[a]

Shell ID	Type	Site of collection	n	SST (°C)					
				Mean	Median	Max	Min	S.D.	Var
B.C.2	Modern	Taltal area	8	15.82	15.49	18.74	14.16	1.59	2.54
B.P6.2	Modern	Taltal area	8	16.53	16.51	18.69	14.03	1.66	2.77
Z.P6.1	Modern	Paposo area	8	16.47	16.53	17.65	15.11	0.92	0.84
Z.P6.2	Modern	Paposo area	8	16.40	16.26	18.25	14.30	1.44	2.09
B.C.P.1	Modern	Taltal area	8	17.33	17.84	19.64	14.49	1.91	3.65
B.C.P.2	Modern	Taltal area	8	17.81	18.30	19.23	14.23	1.63	2.65
L.F.P.1	Modern	Paposo area	8	17.70	17.84	18.45	16.75	0.72	0.51
L.F.P.2	Modern	Paposo area	8	17.93	17.90	19.67	15.32	1.31	1.71
Total modern				16.99	17.29	19.67	14.03	1.55	2.42
A.C.1	Archaeological	Site 224A	8	13.43	13.53	15.01	11.12	1.46	2.14
A.C.2	Archaeological	Site 224A	8	13.36	13.50	14.89	11.29	1.11	1.24
A.C.3	Archaeological	Site 224A	8	13.55	13.24	15.25	12.16	1.23	1.51
A.C.4	Archaeological	Site 224A	7	13.99	14.54	15.16	12.06	1.25	1.56
P.F.1	Archaeological	Site PN9	8	14.51	14.97	15.72	11.89	1.26	1.60
P.F.2	Archaeological	Site PN9	8	13.68	13.88	14.97	11.94	1.08	1.16
P.F.3	Archaeological	Site PN9	8	15.02	15.30	17.42	11.21	1.96	3.82
P.F.4	Archaeological	Site PN9	8	15.52	15.59	18.73	12.25	1.91	3.66
Total archaeological				14.13	14.24	18.73	11.12	1.56	2.44

[a] N refers to the number of samples per shell.

Mediterranean, where reconstructed SST was generally 1 °C warmer than instrumental SST (Prendergast and Schöne, 2017). Explanations provided by Prendergast and Schöne (2017) for warmer reconstructed SST is that water in intertidal habitats of mollusc species may be slightly warmer than that recorded in thermometers or that sampled species may grow during part of the day when temperatures are warmer than instrumental records. This may be our case, since *F. maxima* shells were obtained from the intertidal zone and thermometers were attached to local piers, approximately 1 m below mean low water.

Other factors proposed as mechanisms to explain observed depletion of ^{18}O are shell deposition during changes in the pH of water or during evaporative conditions, or biomineralization processes by respired CO_2 (Fenger et al., 2007; Parker et al., 2017; Spero and Lea, 1996). No information is available on the mechanisms by which *F. maxima* precipitates its shell, and therefore it is not possible to evaluate which factor may explain depleted $\delta^{18}O_{shell}$ values. Evaporative conditions may be ruled out since our *F. maxima* shells were obtained from intertidal areas directly exposed to wave action and not from habitats with enhanced evaporation like tide pools. However, a strong El Niño event was observed along the southeast Pacific between 2015 and 2016 (https://www.esrl.noaa.gov/psd/enso/mei/). This oceanographic condition is likely to have changed water mass characteristics in the coastal zone, including the pH of upwelled water in northern Chile (Ulloa et al., 2001; Vargas et al., 2017). Consequently, it is possible that changes in water pH happened during shell deposition of our *F. maxima* specimens, causing depleted $\delta^{18}O_{shell}$ values.

The mechanisms responsible for ^{18}O enrichment or depletion of biomineralized calcite in shells of *F. maxima* remain unknown, and our data do not provide an accurate calculation of the offset between predicted and measured $\delta^{18}O_{shell}$ values. Subsequently, the 1.1 ± 0.5‰ offset will not be used to reconstruct SST from $\delta^{18}O_{shell}$ values of modern and archaeological *F. maxima* shells. In the meantime, as in situ thermometers are a reliable source of local SST, temperature offset of +1.04°C may be considered as a more dependable parameter to correct reconstructed shell SST. Because this temperature offset is predictable and can be taken into account, reconstructed SST from *F. maxima* $\delta^{18}O_{shell}$ values can be considered a useful proxy for water temperature, with an approximate error of +1.04 °C.

Several species-specific equations have been developed to improve the accuracy of paleotemperature reconstructions from carbonate skeletons (Ford et al., 2010; Wanamaker Jr. et al., 2007). As the development of these equation requires comprehensive studies on the mollusc species under study, many of these equations have been applied to other species (i.e. Carré et al., 2005a, 2005b; Colonese et al., 2012; Galimberti et al., 2017; Jew et al., 2016). In this study we used a paleotemperature equation originally developed for *M. californianus* (Ford et al., 2010) that resulted in a difference of +1.04 °C between mean SST reconstructed from modern *F. maxima* shells and mean SST obtained from in situ thermometers. This highlights the necessity of calibrating the Ford et al. (2010) equation for *F. maxima*. As stated above, given that our shell sampling strategy does not control for shell growth rates or shell microsample chronology, the slope of the paleotemperature equation used to convert *F. maxima* $\delta^{18}O_{shell}$ values (Ford et al., 2010) cannot been tested, thus adding uncertainty to our $\delta^{18}O_{shell}$ derived mean SST results.

Reconstructed SST from modern *F. maxima* shells are different than SST reconstructed from archaeological shells (modern and archaeological $\delta^{18}O_{shell}$ values without the offset correction) dated by association to 11,206 and 11,010 cal yr BP (Figs. 8 and 9, Table 8). Early Holocene mean SST (14.13 °C) was cooler than modern temperatures (shell 16.99 °C, thermometer 15.95 °C) (Table 8). This difference implies that Early Holocene mean SST at 25°S was ~2.86 °C cooler than today. This difference between SST estimates based on modern and archaeological shell samples is statistically significant (*t*-test $p < 0.000$, df = 125). Considering the temperature error of +1.04 °C, corrected mean SST from modern shells would be 15.95 °C and from

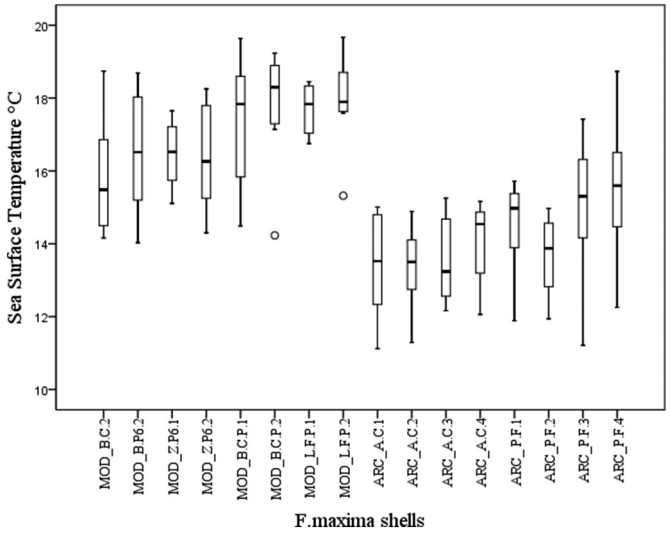

Fig. 8. Boxplots for modern and archaeological shell SST values. Reconstructed SST are on *F. maxima* $\delta^{18}O_{shell}$ values without the offset correction. MOD refers to modern shells and ARC to archaeological shells. Each boxplot represents eight shell carbonate samples, except for archaeological shell A.C.4 with only seven samples. Outlier value from this shell is not included.

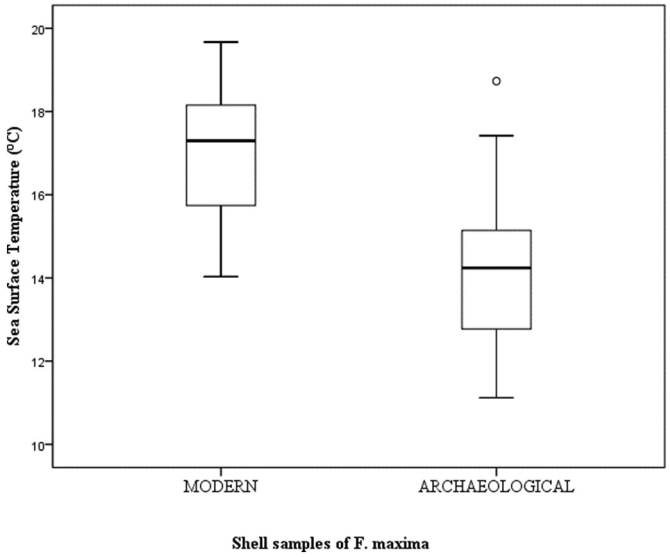

Fig. 9. Boxplot for overall modern and archaeological shell SST values. Reconstructed SST are on *F. maxima* $\delta^{18}O_{shell}$ values without the offset correction. MODERN refers to modern samples (n = 64) and ARCHAEOLOGICAL to archaeological samples (n = 63).

archaeological shells 13.09 °C. This correction maintains the pattern observed of 2.86 °C difference between modern and archaeological mean SST around the Paposo and Taltal areas.

Early Holocene SST reconstructed from archaeological *F. maxima* shells suggests cold SST around the area. Modern conditions associated with nearshore cold waters along the coast of Chile are associated with upwelling activity and entail high primary productivity, the presence of large kelp beds (Vásquez et al., 1998; Villegas et al., 2007) and characteristic associated fauna dominated by benthic species such as herbivorous fishes and a diverse molluscan assemblage (Aldana et al., 2017; Reddin et al., 2015; Wieters, 2005). This scenario is complementary to paleoclimate reconstructions for inland and littoral terrestrial environments that attest to increased local humidity brought about by increased groundwater recharge in inland Andean catchments and/or increased intensity of coastal fog (Díaz et al., 2012; Saez et al.,

2016). The cold and humid climate pattern during the Pleistocene–Holocene transition is detected over much of the Atacama desert and has been attributed to oceanographic and atmospheric anomalies induced by prevailing La Niña–like conditions in the Tropical Pacific (Gayo et al., 2012a, 2012b; Latorre et al., 2002; Maldonado et al., 2005; Quade et al., 2008; Saez et al., 2016).

Early human occupations made use of these favourable environmental conditions, effectively adapting to both highland and coastal ecosystems as early as 11,800 cal yr BP (Cartajena et al., 2014; Grosjean et al., 2005; Latorre et al., 2013; Llagostera, 1992, 2005; Llagostera et al., 2000; Núñez et al., 2002; Salazar et al., 2011, 2017). Marine faunal remains from archaeological sites 224A and Paposo Norte 9 support the scenario of productive habitats along the coast of Taltal. Archaeological fauna assemblages from these sites are characterized by high abundance of different species of the genus *Fissurella* (keyhole limpet), *Acanthopleura echinata* (chiton), *Enoplochiton niger* (chiton), *Tegula atra* (sea snail), and *C. concholepas* shells (Olguín et al., 2015a; Salazar et al., 2017). Regarding fish species, ichthyofaunal records show a predominance of species like *Sciaena deliciosa*, *Cilus gilberti*, *Semicossyphus darwini*, *Scartichthys viridis* and *Trachurus murphyi* (Rebolledo et al., 2016; Salazar et al., 2017), most of them cold water kelp–forest fishes (Berrios and Vargas, 2000; Pérez-Matus et al., 2012). It is interesting to note that archaeological sites from the study area with dates later than 8500 cal yr BP have ichthyofaunal assemblages with higher abundance of warmer water species (Rebolledo et al., 2016). Further studies will be necessary to evaluate the role of paleoceanographic conditions on the composition of fish remains from Middle Holocene archaeological sites of the area of Taltal and the northern coast of Chile.

Our results point to colder than present nearshore conditions during the Early Holocene that are consistent with previous sea temperature reconstructions. Isotope studies ($\delta^{18}O$) on *C. concholepas* shells from La Chimba–13 archaeological site (23°S) – two degrees of latitude north of our study area and with dates between 10,550 and 9120 cal yr BP – show that coastal SST was around 4 °C cooler than present (Vargas et al., 2006). These similarities coincide with previous interpretations of prevailing cooler SST during the Early Holocene on the coast of southern Peru (18°S) between 9600 and 8900 cal BP (Carré et al., 2005a, 2014).

Reconstructed shell SST from central Chile (31°S) between 10,380 and 9460 cal yr BP have been reported to be similar to modern SST values (Carré et al., 2012). Several explanations have been proposed to interpret higher SST and lower reservoir ages than those obtained in southern Peru and northern Chile (15°S to 23°S) during the Early Holocene (Carré et al., 2016; Fontugne et al., 2004; Ortlieb et al., 2011). This Early Holocene latitudinal contrast has been interpreted as the result of differences in the intensity of the upwelling activity along the northern coast (Carré et al., 2005a, 2014; Sadler et al., 2012), a difference in the ^{14}C content of upwelled waters due to their origin (for example higher or lower contribution of sub-Antarctic mode waters (SAMW)) (Fontugne et al., 2004; Hua et al., 2015), and/or the result of changes in the latitudinal character of air-sea CO_2 exchange due to the location of the ESSW–SAMW front somewhere between northern (~18°S) and central Chile (31°S) (Carré et al., 2016).

As deep water brought to the surface by coastal upwelling is characterized by lower temperatures (Aravena et al., 2014; Thiel et al., 2007), Early Holocene cooler SST (Carré et al., 2005a, 2014) and high marine reservoir ages are interpreted as increased upwelling intensity (Carré et al., 2016) on the southern coast of Peru (18°S), which suggests that the cooler than present SST recorded for archaeological shells from sites 224A and Paposo Norte 9 (Taltal, 25°S) and from La Chimba–13 (23°S) may be related to high upwelling activity in the area. More information on reconstructed SST and radiocarbon marine reservoir ages is needed to evaluate and explain changes in paleoceanographic conditions throughout the Holocene along the northern coast of Chile (from 18 to 31°S). Nevertheless, paleo–SST data from archaeological shells of Taltal contribute to decrease the uncertainty on the spatial organization of paleoceanographic patterns during the Early Holocene. Between around 11,000 and 9000 cal yr BP, the area from southern Peru (18°S) to Taltal (25°S) was characterized by cooler waters and strong upwelling, while the area around Los Vilos (31°S) was dominated by warmer waters and weaker upwelling. These spatial patterns suggest that Early Holocene human occupations of the coast of southern Peru to northern Chile experienced an environment that was distinctively influenced by strong upwelling conditions.

8. Conclusions

In the present study we have provided the first SST record from $\delta^{18}O$ analyses on modern and archaeological shell carbonates for the coastal Atacama desert (area of Taltal, 25°S). In addition, we have presented the first isotope study on a keyhole limpet species (*F. maxima*) from the Pacific coast of South America, and the first XDR on the composition of calcium carbonate of its shell. Finally, we have calibrated reconstructed SST from modern shells of *F. maxima* with in situ SST measurements for the study area. Mean SST value recorded in thermometers is around 0.93 °C lower than mean SST from satellite information. Therefore, in cases when in situ thermometers are not available to compare with reconstructed shell SST, this offset has to be considered. The reconstructed mean SST obtained from $\delta^{18}O$ values on calcite outer layers of modern *F. maxima* shells is 1.04 °C warmer than the mean SST from in situ thermometers. Because this temperature offset is predictable and can be taken into account, reconstructed SST from *F. maxima* $\delta^{18}O_{shell}$ values can be considered a useful proxy for water temperature, with an approximate error of +1.04 °C. Our results confirm paleoceanographic patterns previously reported for the Early Holocene along South America, with cooler nearshore waters and strong upwelling along the southern coast of Peru and northern Chile. These data are crucial to understand the environmental context of early peopling of the coast of the Atacama desert and South America. Further experimental studies are needed on *F. maxima* shells to assess, for example, the influence of temperature thresholds on its biological processes and during active mineralization. In this regard, sclerochronology studies are needed to identify shell microsample chronology and growth rate of this shellfish species, ubiquitous in shell midden sites along the coast of Chile. Finally, additional studies should be conducted between Taltal (25°S) and Los Vilos (31°S) to identify the past location of the ESSW–SAMW front and therefore understand temporal changes in the structure of the Humboldt Current along the Holocene and their influence on human adaptation through the prehistory of South America.

Supplementary data to this article can be found online at https://doi.org/10.1016/j.palaeo.2018.03.031.

Acknowledgements

Funding: This work was supported by the National Fund for Scientific and Technological Development (FONDECYT #1151203, 11150210, 3170913, 1181300); and the Fund for Research Centers in Priority Areas (FONDAP/CONICYT 151100 (to CR^2)). Special thanks to Laura Farías, Marcelo Rivadeneira and Patricio Manríquez for their support during shell sample processing (lab space and analytical tools). Thanks to Macarena Troncoso; to Heather Thakar for her comments and help, to Laura Olguín for helping gathering shell samples, and Matthieu Carré for his help regarding ice sheet corrections. We also acknowledge the Faculty of Environmental Sciences of the Universidad de Concepción for hosting a sabbatical leave that was supported by the Millenium Scientific Initiative through the Center for the Study Multiple Drivers on Marine Socio–Ecological Systems (MUSELS). Finally, we are thankful to Mario Vallejos and Leopoldo González from Taltal and Paposo, who helped to collect modern samples of *F. maxima* shells and to install in situ thermometers.

References

Aharon, P., Chappell, J., 1986. Oxygen isotopes, sea level changes and the temperature history of a coral reef environment in New Guinea over the last 105 years. Palaeogeogr. Palaeoclimatol. Palaeoecol. 56, 337–379.

Aldana, M., García-Huidobro, M.R., Pulgar, V.M., Pulgar, J., 2017. Upwelling promotes earlier onset and increased rate of gonadal development of four coastal herbivores. Bull. Mar. Sci. 93 (3), 671–688.

Aravena, G., Broitman, B.R., Stenseth, N.C., 2014. Twelve years of change in coastal upwelling along the central–northern coast of Chile: spatially heterogeneous responses to climatic variability. PLoS One 9 (2), e90276. http://dx.doi.org/10.1371/journal.pone.0090276.

Arroyo, M., Squeo, F.A., Armesto, J., Villagrán, C., 1988. Effects of aridity on plant diversity in the Northern Chilean Andes: results of a natural experiment. Ann. Mo. Bot. Gard. 75, 55–78.

Bailey, G., Deith, M., Shackleton, N., 1983. Oxygen isotope analysis and seasonality determinations: limits and potential of a new technique. Am. Antiq. 48 (2), 390–398.

Barber, R., Chavez, F., 1983. Biological consequences of El Niño. Science 222, 1203–1210.

Béarez, P., Fuentes-Mucherl, F., Rebolledo, S., Salazar, D., Olguín, L., 2016. Billfish foraging along the Northern coast of Chile during the Middle Holocene (7400–5900 cal BP). J. Anthropol. Archaeol. 41, 185–195.

Berrios, V., Vargas, M., 2000. Estructura del ensamble de peces intermareales de la costa rocosa del norte de Chile. Rev. Biol. Mar. Oceanogr. 35 (1), 73–81.

Bijma, J., Spero, H.J., Lea, D.W., 1999. Reassessing foraminiferal stable isotope geochemistry: impact of the oceanic carbonate system (experimental results). In: Fischer, G., Wefer, G. (Eds.), Uses of Proxies in Paleoceanography: Examples From the South Atlantic. Springer-Verlag, Berlin, pp. 489–512.

Bretos, M., 1982. Biología de *Fissurella maxima* Sowerby (Mollusca: Archaeogastropoda) en el norte de Chile. 1. Caracteres generales, edad y crecimiento. Cah. Biol. Mar. 23, 159–170.

Bretos, M., Tesorieri, I., Alvarez, L., 1983. The biology of *Fissurella maxima* Sowerby (Mollusca: Archaeogastropoda) in Northern Chile. 2. Notes on its reproduction. Biol. Bull. 165, 559–568.

Broitman, B.R., Navarrete, S.A., Smith, F., Gaines, S.D., 2001. Geographic variation of Southeastern Pacific intertidal communities. Mar. Ecol. Prog. Ser. 224, 21–34.

Carré, M., Bentale, I., Fontugne, M., Lavallée, D., 2005a. Strong El Niño events during the early Holocene: stable isotope evidence from Peruvian sea–shells. The Holocene 15, 42–47.

Carré, M., Bentaleb, I., Blamart, D., Ogle, N., Cardenas, F., Zevallos, S., Kalin, R.M., Ortlieb, L., Fontugne, M., 2005b. Stable isotopes and sclerochronology of the bivalve *Mesodesma donacium*: potential application to Peruvian paleoceanographic reconstructions. Paleogeogr. Paleoclimatol. Paleoecol. 228, 4–25.

Carré, M., Azzoug, M., Bentaleb, I., Chase, B.M., Fontugne, M., Jackson, D., Ledru, M.P., Maldonado, A., Sachs, J.P., Schauer, A.J., 2012. Mid–Holocene mean climate in the South–eastern Pacific and its influence on South America. Quat. Int. 253, 55–66.

Carré, M., Sachs, J.P., Purca, S., Schauer, A.J., Braconnot, P., Angeles Falcón, R., Julien, M., Lavallée, D., 2014. Holocene history of ENSO variance and asymmetry in the eastern tropical Pacific. Science 345, 1045–1048.

Carré, M., Jackson, D., Maldonado, A., Chase, B.M., Sachs, J.P., 2016. Variability of 14C reservoir age and air–sea flux of CO2 in the Peru–Chile upwelling region during the past 12,000 years. Quat. Res. 85, 87–93.

Cartajena, I., Loyola, R., Núñez, L., Faúndez, W., 2014. Problemas y perspectivas en la interpretación del registro espacial de Punta Negra–Imilac. In: Falabella, F., Sanhueza, L., Cornejo, L., Correa, I. (Eds.), Distribución espacial en sociedades no aldeanas. Del registro arqueológico a la interpretación social. Monografías de la Sociedad Chilena de Arqueología 4, Santiago, pp. 143–162.

Cereceda, P., Larrain, H., Osses, P., Farías, M., Egaña, I., 2008. The climate of the coast and fog zone in the Tarapacá Region, Atacama Desert, Chile. Atmos. Res. 87, 301–311.

Chavez, F., Bertrand, A., Guevara-Carrasco, R., Soler, P., Csirke, J., 2008. The Northern Humboldt Current System: brief history, present status and a view towards the future. Prog. Oceanogr. 79, 95–105. http://dx.doi.org/10.1016/j.pocean.2008.10.012.

Cohen, A.L., Tyson, P.D., 1995. Sea–surface temperature fluctuations during the Holocene off the south coast of Africa: implications for terrestrial climate and rainfall. The Holocene 5 (3), 304–312.

Colonese, A.C., Verdún-Castelló, E., Álvarez, M., Briz i Godino, I., Zurro, D., Salvatelli, L., 2012. Oxygen isotopic composition of limpet shells from the Beagle Channel: implications for seasonal studies in shell middens of Tierra del Fuego. J. Archaeol. Sci. 39, 1738e1748.

Díaz, F., Latorre, C., Maldonado, A., Quade, J., Betancourt, J.L., 2012. Rodent middens reveal episodic, long distance plant colonizations across the hyperarid Atacama Desert over the last 34,000 years. J. Biogeogr. 39, 510–525.

Duplessy, J.C., Labeyrie, L., Waelbroeck, C., 2002. Constraints on the ocean oxygen isotopic enrichment between the Last Glacial Maximum and the Holocene: paleoceanographic implications. Quat. Sci. Rev. 21 (1–3), 315–330.

Falabella, F., Planella, M.T., Pollastri, A., 1991. Análisis de Oxígeno 18 en material malacológico de Chile Central. In: Proceeding XI Congreso Nacional de Arqueología Chilena, 3. Museo Nacional de Historia Natural y Sociedad Chilena de Arqueología, Santiago, pp. 95–112.

Fenger, T., Surge, D., Schöne, B., Milner, N., 2007. Sclerochronology and geochemical variation in limpet shells (*Patella vulgata*): a new archive to reconstruct coastal sea surface temperature. Geochem. Geophys. Geosyst. 8 (7), Q07001. http://dx.doi.org/10.1029/2006GC001488.

Ferguson, J.E., Henderson, G.M., Fa, D.A., Finlayson, J.C., Charnley, N.R., 2011. Increased seasonality in the Western Mediterranean during the last glacial from limpet shell geochemistry. Earth Planet. Sci. Lett. 308, 325–333.

Flores, C., 2017. Importance of small–scale paleo–oceanographic conditions to interpret changes in size of California mussel (*Mytilus californianus*). Late Holocene, Santa Cruz island, California. Quat. Int. 427, 137–150.

Fontugne, M., Carré, M., Bentaleb, I., Julien, M., Lavallée, D., 2004. Radiocarbon reservoir age variations in the South Peruvian upwelling during the Holocene. Radiocarbon 46, 531–537.

Ford, H.L., Schellenberg, S.A., Becker, B.J., Deutschman, D.L., Dyck, K.A., Koch, P.L., 2010. Evaluating the skeletal chemistry of *Mytilus californianus* as a temperature proxy: effects of microenvironment and ontogeny. Paleoceanography 25 (1), PA1203. http://dx.doi.org/10.1029/2008PA001677.

Friedman, I., O'Neil, J.R., 1997. Compilation of stable isotope fractionation factors of geochemical interest. In: Geol. Surv. Prof. Pap. 440KK. US Govt. Printing Office.

Galimberti, M., Loftus, E., Sealy, J., 2017. Investigating δ18O of *Turbo sarmaticus* (L. 1758) as an indicator of sea surface temperatures. Palaeogeogr. Palaeoclimatol. Palaeoecol. 484, 62–69.

Garreaud, R., Vuille, M., Clement, A., 2003. The climate of the Altiplano: observed current conditions and mechanisms of past changes. Palaeogeogr. Palaeoclimatol. Palaeoecol. 194, 5–22.

Garreaud, R., Barichivich, J., Christie, D.A., Maldonado, A., 2008. Interannual variability of the coastal fog at Fray Jorge relict forests in semiarid Chile. J. Geophys. Res. 113, 1–16.

Gayo, E.M., Latorre, C., Jordan, T.E., Nester, P.L., Estay, S.A., Ojeda, K.F., Santoro, C.M., 2012a. Late Quaternary hydrological and ecological changes in the hyperarid core of the Northern Atacama Desert (~21_S). Earth Sci. Rev. 113, 120–140.

Gayo, E.M., Latorre, C., Santoro, C.M., Maldonado, A., De Pol-Holz, R., 2012b. Hydroclimate variability in the low–elevation Atacama Desert over the last 2500 years. Clim. Past 8, 287–306.

Glassow, M.A., Thakar, H.B., Kennett, D.J., 2012. Red abalone collecting and marine water temperature during the middle Holocene occupation of Santa Cruz Island, California. J. Archaeol. Sci. 39, 2574–2582.

Grosjean, M., Núñez, L., Cartajena, I., 2005. Palaeoindian occupation of the Atacama Desert, Northern Chile. J. Quat. Sci. 20, 643–653.

Grossman, E.L., Ku, T.L., 1986. Oxygen and carbon fractionation in biogenic aragonite: temperature effect. Chem. Geol. 59, 59–74.

Gutiérrez-Zugasti, I., Suárez-Revilla, R., Clarke, L.J., Schöne, B.R., Bailey, G.B., González-Morales, M.R., 2017. Shell oxygen isotope values and sclerochronology of the limpet *Patella vulgata* Linnaeus 1758 from Northern Iberia: implications for the reconstruction of past seawater temperatures. Palaeogeogr. Palaeoclimatol. Palaeoecol. 475, 162–175.

Herrera, C., Custodio, E., 2014. Origin of waters from small springs located at the Northern coast of Chile, in the vicinity of Antofagasta. Andean Geol. 41 (2), 314–341.

Herrera, C., Gamboa, C., Custodio, E., Jordan, T., Godfrey, L., Jódar, J., Luque, J.A., Vargas, J., Sáez, A., 2018. Groundwater origin and recharge in the hyperarid Cordillera de la Costa, Atacama Desert, northern Chile. Sci. Total Environ. 624, 114–132.

Houston, J., 2006. Variability of precipitation in the Atacama Desert: its causes and hydrological impact. Int. J. Climatol. 26, 2181–2198.

Hua, Q., Webb, G.E., Zhao, J.X., Nothdurft, L.D., Lybolt, M., Price, G.J., Opdyke, B.N., 2015. Large variations in the Holocene marine radiocarbon reservoir effect reflect ocean circulation and climatic changes. Earth Planet. Sci. Lett. 422, 33–44.

Ibaraki, M., 1997. Closing of the Central American Seaway and Neogene coastal upwelling along the Pacific coast of South America. Tectonophysics 281, 99–104. http://dx.doi.org/10.1016/S0040–1951(97)00161–3.

Jerardino, A., Navarro, R., 2008. Shell morphometry of seven limpet species from coastal shell middens in southern Africa. J. Archaeol. Sci. 35, 1023–1029.

Jew, N.P., Fitzpatrick, S.M., Sullivan, K.J., 2016. $\delta^{18}O$ analysis of *Donax denticulatus*: evaluating a proxy for sea surface temperature and nearshore paleoenvironmental reconstructions for the northern Caribbean. J. Archaeol. Sci. Rep. 8, 216–223.

Keith, M.L., Anderson, G.M., Eichler, R., 1964. Carbon and oxygen isotopic composition of mollusc shells from marine and fresh–water environments. Geochim. Cosmochim. 28 (10 − 11), 1757–1786.

Kim, J.H., Schneider, R.R., Hebbeln, D., Muller, P.J., Wefer, G., 2002. Last deglacial sea–surface temperature evolution in the Southeast Pacific compared to climate changes on the South American continent. Quat. Sci. Rev. 21, 2085–2097.

Lambeck, K., Chappell, J., 2001. Sea level change through the last glacial cycle. Science 292, 679–686.

Latorre, C., Betancourt, J.L., Rylander, K., Quade, J., 2002. Vegetation invasions into absolute desert: a 45 000 yr rodent midden record from the Calama–Salar de Atacama basins, Northern Chile (lat 22°–24°S). Geol. Soc. Am. Bull. 114, 349–366.

Latorre, C., Santoro, C., Ugalde, P., Gayo, E., Osorio, D., Salas-Egaña, C., De Pol-Holz, R., Joly, D., Rech, J., 2013. Late Pleistocene human occupation of the hyperarid core in the Atacama Desert, northern Chile. Quat. Sci. Rev. 77, 19–30.

Latorre, C., De Pol-Holz, R., Carter, C., Santoro, C.M., 2017. Using archaeological shell middens as a proxy for past local coastal upwelling in Northern Chile. Quat. Int. 427, 128–136.

Llagostera, A., 1992. Early occupations and the emergence of fishermen on the Pacific Coast of South America. Andean Past. 3, 87–109.

Llagostera, A., 2005. Culturas costeras precolombinas en el norte chileno: secuencia y subsistencia de las poblaciones arcaicas. In: Figueroa, E. (Ed.), Biodiversidad marina: valoración, usos, perspectivas ¿Hacia dónde va Chile? Editorial Universitaria, Santiago, Chile, pp. 107–148.

Llagostera, A., Weisner, R., Castillo, G., Cervellino, M., Costa-Junquera, M., 2000. El Complejo Huentelauquen bajo una perspectiva macroespacial y multi–disciplinaria. In: Actas de XIV Congreso Nacional de Arqueología Chilena. Copiapó, Chile, pp.

461–482.
Maldonado, A., Betancourt, J.L., Latorre, C., Villagran, C., 2005. Pollen analyses from a 50 000-yr rodent midden series in the southern Atacama Desert (25°30′S). J. Quat. Sci. 20 (5), 493–507.
Mannino, M.A., Thomas, K.D., Leng, M.J., Sloane, H.J., 2008. Shell growth and oxygen isotopes in the topshell *Osilinus turbinatus*: resolving past inshore sea surface temperatures. Geo-Mar. Lett. 28, 309–325.
Marquet, P.A., Bozinovic, F., Bradshaw, G.A., Cornelius, C., Gonzalez, H., Gutierrez, J.R., Hajek, E.R., Lagos, J.A., López-Cortes, F., Nuñez, L., Rosello, E.F., Santoro, C., Samaniego, H., Standen, V.G., Torres-Mura, J.C., Jaksic, F.M., 1998. Los ecosistemas del Desierto de Atacama y área Andina adyacente. Rev. Chil. Hist. Nat. 71, 593–617.
McConnaughey, T., 1989. 13C and 18O isotopic disequilibrium in biological carbonates: II. In vitro simulation of kinetic isotope effects. Geochim. Cosmochim. Acta 53 (1), 163–171.
McLean, J.H., 1984. Systematics of *Fissurella* in the Peruviana and Magellanic faunal provinces (Gastropoda: Prosobranquia). In: Contributions in Science, Natural History Museum of Los Angeles County. 354. pp. 1–70.
Mohtadi, M., Romero, O.E., Hebbeln, D., 2004. Changing marine productivity off Northern Chile during the past 19 000 years: a multivariable approach. J. Quat. Sci. 19 (4), 347–360.
Montecino, V., Strub, P.T., Chavez, F.P., Thomas, A.C., Tarazona, J., Baumgartner, T., 2005. In: Robinson, A.R., Brink, K.H. (Eds.), Bio-physical interactions off western South America. The Sea. Harvard University Press, Cambridge, pp. 329–390.
Nielsen, K., Navarrete, S., 2004. Mesoscale regulation comes from the bottom–up: intertidal interactions between consumers and upwelling. Ecol. Lett. 7, 31–41.
Núñez, L., Grosjean, M., Cartajena, I., 2002. Human occupations and climate change in the Puna de Atacama, Chile. Science 298, 821–824.
Olguín, L., Salazar, D., Jackson, D., 2014. Tempranas evidencias de navegación y caza de especies oceánicas en la costa pacífica de sudamérica (Taltal, ~7.000 años cal. A.P.) Chungara. 46. pp. 177–192.
Olguín, L., Flores, C., Salazar, D., 2015a. Aprovechamiento humano de moluscos marinos en conchales arqueológicos del Holoceno Temprano y Medio (12.000–5.000 años cal A.P.). Costa meridional del Desierto de Atacama. Chile. In: Hammond, H., Zubimendi, M.A. (Eds.), Arqueomalacología: abordajes metodológicos y casos de estudio en el Cono Sur. Fundación de Historia Natural Félix de Azara, Buenos Aires, pp. 13–34.
Olguín, L., Castro, V., Peña-Villalobos, I., Ruz, J., Santander, B., 2015b. Exploitation of faunal resources by marine hunter gatherer groups during the Middle Holocene at the Copaca 1 site, Atacama Desert coast. Quat. Int. 373, 4–16.
Ortlieb, L., Vargas, G., Saliege, J.F., 2011. Marine radiocarbon reservoir effect along the northern Chile–southern Peru coast (14–24°S) throughout the Holocene. Quat. Res. 75, 91–103.
Osorio, C., Ramirez, M.E., Salgado, J., 1988. Gastric content of *Fissurella maxima* (Mollusca: Archaeogastropoda) at Los Vilos, Chile. Veliger 30 (4), 347–350.
Owen, R., Kennedy, H., Richardson, C., 2002. Experimental investigation into partitioning of stable isotopes between scallop (*Pecten maximus*) shell calcite and sea water. Palaeogeogr. Palaeoclimatol. Paleoecol. 185, 163–174.
Parker, W.G., Yanes, Y., Surge, D., Mesa-Hernández, E., 2017. Calibration of the oxygen isotope ratios of the gastropods *Patella candei crenata* and *Phorcus atratus* as high-resolution paleothermometers from the subtropical eastern Atlantic Ocean. 2017. Palaeogeogr. Palaeoclimatol. Palaeoecol. 487, 251–259.
Pérez-Matus, A., Pledger, S., Díaz, F., Ferry, L., Vásquez, J.A., 2012. Plasticity in feeding selectivity and trophic structure of kelp forest associated fishes from Northern Chile. Rev. Chil. Hist. Nat. 85, 29–48.
Prendergast, A.L., Schöne, B.R., 2017. Oxygen isotopes from limpet shells: implications for palaeothermometry and seasonal shellfish foraging studies in the Mediterranean. Palaeogeogr. Palaeoclimatol. Palaeoecol. 484, 33–47.
Prendergast, A.L., Azzopardi, M., O'Connell, T.C., Hunt, C., Barker, G., Stevens, R.E., 2013. Oxygen isotopes from *Phorcus* (*Osilinus*) *turbinatus* shells as a proxy for sea surface temperature in the central Mediterranean: a case study from Malta. Chem. Geol. 345, 77–86.
Quade, J., Rech, J.A., Betancourt, J.L., Latorre, C., Quade, B., Rylander, K.A., Fisher, T., 2008. Paleowetlands and regional climate change in the central Atacama Desert, Northern Chile. Quat. Res. 69, 343–360.
Rebolledo, S., Béarez, P., Salazar, D., Fuentes, F., 2016. Maritime fishing during the Middle Holocene in the hyperarid coast of the Atacama Desert. Quat. Int. 391, 3–11.
Reddin, C.J., Docmac, F., O'Connor, N.E., Bothwell, J.H., Harrod, C., 2015. Coastal upwelling drives intertidal assemblage structure and trophic ecology. PLoS One 10 (7), e0130789.
Reitz, E.J., deFrance, D., Sandweiss, D.H., McInnis, H.E., 2015. Flexibility in southern Peru coastal economies: a vertebrate perspective on the Terminal Pleistocene/Holocene transition. J. Island Coast. Archaeol. 10, 155–183.
Reitz, E.J., McInnis, H.E., Sandweiss, D.H., deFrance, D., 2016. Variations in human adaptations during the Terminal Pleistocene and Early Holocene at Quebrada Jaguay (QJ–280) and the Ring Site, southern Peru. J. Island Coast. Archaeol. 12, 224–254.
Rundel, P.W., Dillon, M.O., Palma, B., Mooney, H.A., Gulmon, S.L., Ehleringer, J.R., 1991. The phytogeography and ecology of the coastal Atacama and Peruvian deserts. Aliso 13, 1–49.
Sadler, J., Carré, M., Azzoug, M., Schauer, A.J., Ledesma, J., Cardenas, F., Chase, B.M., Bentaleb, I., Muller, S.D., Mandeng, M., Rohling, E.J., Sachs, J.P., 2012. Reconstructing past upwelling intensity and the seasonal dynamics of primary productivity along the Peruvian coastline from mollusk shell stable isotopes. Geochem. Geophys. Geosyst. 13, Q01015.
Saez, A., Godfrey, L.V., Herrera, C., Chong, G., Pueyo, J., 2016. Timing of wet episodes in Atacama Desert over the last 15 ka. The Groundwater Discharge Deposits (GWD) from Domeyko Range at 25°S. Quat. Sci. Rev. 145, 82–93.
Salazar, D., Jackson, D., Guendon, J.L., Salinas, H., Morata, D., Figueroa, V., Manríquez, G., Castro, V., 2011. Early evidence (ca. 12,000 BP) for iron oxide mining on the Pacific coast of South America. Curr. Anthropol. 52, 463–475.
Salazar, D., Andrade, P., Escobar, M., Figueroa, V., Flores, C., Olguín, L., Salinas, H., 2013. Nuevos sitios correspondientes al complejo cultural Huentelauquén en la costa de Taltal. Taltalia. 5–6. pp. 9–19.
Salazar, D., Figueroa, V., Andrade, P., Salinas, H., Power, X., Rebolledo, S., Parra, S., Orellana, H., Urrea, J., 2015. Cronología y organización económica de las poblaciones arcaicas de la costa de Taltal. Estudios Atacameños. 50. pp. 7–46.
Salazar, D., Arenas, C., Andrade, P., Olguín, L., Torres, J., Flores, C., Vargas, G., Rebolledo, S., Borie, C., Sandoval, C., Silva, C., Delgado, A., Lira, N., Robles, C., 2017. From the use of space to territorialisation during the Pleistocene–Holocene transition in Taltal, coastal Atacama Desert, Chile. Quat. Int. http://dx.doi.org/10.1016/j.quaint.2017.09.035. In Press.
Santoro, C.M., Gayo, E.M., Carter, C., Standen, V.G., Castro, V., Valenzuela, D., De Pol-Holz, R., Marquet, P.A., Latorre, C., 2017. Loco or no Loco? Holocene climatic fluctuations, human demography, and community based management of coastal resources in Northern Chile. Front. Earth Sci. 5 (77). http://dx.doi.org/10.3389/feart.2017.00077.
Schifano, G., Censi, P., 1983. Oxygen isotope composition and rate of growth of *Patella coerulea*, *Monodonta turbinata* and *M. articulata* shells from the western coast of Sicily. Palaeogeogr. Palaeoclimatol. Palaeoecol. 42 (3–4), 305–311.
Schöne, B.R., 2008. The curse of physiology – challenges and opportunities in the interpretation of geochemical data from mollusc shells. Geo-Mar. Lett. 28 (5–6), 269–285.
Spero, H.J., Lea, D.W., 1996. Experimental determination of stable isotope variability in *Globigerina bulloides*: implications for paleoceanographic reconstructions. Mar. Micropaleontol. 28 (3), 231–246.
Surge, D., Barrett, J.H., 2012. Marine climatic seasonality during medieval times (10th to 12th centuries) based on isotopic records in Viking Age shells from Orkney, Scotland. Palaeogeogr. Palaeoclimatol. Palaeoecol. 350–352, 236–246.
Thakar, H., 2016. Foraging ancient landscapes: seasonal and spatial variation in prehistoric exploitation of plant and animal food resources on Santa Cruz Island, California. J. Calif. Gt. Basin Anthropol. 36 (1), 27–50.
Thiel, M., Macaya, E.C., Acuña, E., Arntz, W., Bastias, H., Brokordt, K., Camus, P., Castilla, J.C., Castro, L., Cortés, M., Dumont, C., Escribano, R., Fernandez, M., Gajardo, J., Gaymer, C., Gómez, I., González, A., Gonzalez, H., Haye, P., Illanes, J.E., Iriarte, J.L., Lancellotti, D., Luna-Jorquera, G., Luxoro, C., Manriquez, P., Marín, V., Muñoz, P., Navarrete, S.A., Perez, E., Poulin, E., Sellanes, J., Sepúlveda, H., Stotz, W., Tala, F., Thomas, A., Vargas, C., Vásquez, J., Vega, A., 2007. The Humboldt Current System of Northern and Central Chile, oceanographic processes, ecological interactions and socioeconomic feedback. Oceanogr. Mar. Biol. 45, 195–344.
Ulloa, O., Escribano, R., Hormazabal, R., Quiñones, R.A., Gonzalez, R.R., Ramos, M., 2001. Evolution and biological effects of the 1997–98 El Niño in the upwelling ecosystem off northern Chile. Geophys. Res. Lett. 28, 1591–1594.
Valdivia, N., Gonzalez, A., Manzur, T., Broitman, B.R., 2013. Mesoscale variation of mechanisms contributing to stability in rocky shore communities. PLoS One 8 (1), e54159.
Vargas, G., Rutllant, J., Ortlieb, L., 2006. ENSO tropical–extratropical climate teleconnections and mechanisms for Holocene debris flows along the hyperarid coast of western South America (17°–24°S). Earth Planet. Sci. Lett. 249, 467–483.
Vargas, G., Lagos, N.A., Lardies, M.A., Duarte, C., Manriquez, P.H., Aguilera, V.M., Broitman, B., Widdicombre, S., Dupont, S., 2017. Species–specific responses to ocean acidification should account for local adaptation and adaptive plasticity. Nat. Ecol. Evol. 1, 0084. http://dx.doi.org/10.1038/s41559-017-0084.
Vásquez, J.A., Camus, P.A., Ojeda, P., 1998. Diversidad, estructura y funcionamiento de ecosistemas costeros rocosos del norte de Chile. Rev. Chil. Hist. Nat. 71, 479–499.
Villegas, M.J., Laudien, J., Sielfeld, W., Arntz, W.E., 2007. *Macrocystis integrifolia* and *Lessonia trabeculata* (Laminariales; Phaeophyceae) kelp habitat structures and associated macrobenthic community off Northern Chile. Helgol. Mar. Res. 62 (1), 33–43.
Wanamaker Jr., A.D., Kreutz, K.J., Borns Jr., H.W., Introne, D.S., Feindel, S., Funder, S., Rawson, P.D., Barber, B.J., 2007. Experimental determination of salinity, temperature, growth, and metabolic effects on shell isotope chemistry of *Mytilus edulis* collected from Maine and Greenland. Paleoceanography 22, PA2217. http://dx.doi.org/10.1029/2006PA001352.
Wefer, G., Berger, W., 1991. Isotope paleontology: growth and composition of extant calcareous species. Mar. Geol. 100, 207–248.
Wieters, E.A., 2005. Upwelling control of positive interactions over mesoscales: a new link between bottom–up and top–down processes on rocky shores. Mar. Ecol. Prog. Ser. 301, 43–54.
Wilbur, K.M., Owen, G., 1964. Growth. In: Wilbur, K.M., Yonge, C.M. (Eds.), Physiology of Mollusca. 1. Academic Press, New York, pp. 211–242.
Wilcox, A.C., Escauriaza, C., Agredano, R., Mignot, E., Zuazo, V., Otárola, S., Castro, L., Gironás, J., Cienfuegos, R., Mao, L., 2016. An integrated analysis of the March 2015 Atacama floods. Geophys. Res. Lett. 43, 8035–8043.